Canada Basin hydrography in the CESM-LE and observations: implications for vertical ocean heat transport in a transitioning sea ice cover

Juliette Lavoie, Department of Atmospheric and Oceanic Sciences

McGill University, Montreal

May, 2021

A thesis submitted to McGill University in partial fulfillment of the requirements of the degree of

Master of Science

Abstract

In recent years, there has been a significant sea ice retreat in the Pacific sector of the Arctic. One possible cause is the increase in ocean heat flux amplified by the ice-albedo feedback. This paper looks at vertical ocean heat transport from waters of Pacific origin and solar heat into the mixed layer and their impact on the sea ice mass balance in the Community Earth System Model - Large Ensemble (CESM-LE). To this end, we focus on two specific periods with observational hydrographic data from the Arctic Ice Dynamics Joint Experiment (1975-76) and Ice-Tethered Profiler (2004-2018). A comparison between simulated and observed salinity and potential temperature profiles highlights two key model biases in all ensemble members: an absence of Pacific Waters in the water column and a deepening of the winter mixed layer in opposition to observations that show a reduction in depth of the mixed layer and a stronger increase in stratification. Results from a one-dimensional vertical heat budget show that remnant solar heat trapped beneath the halocline is mostly ventilated to the surface by mixing before the following melt season, while vertical advection associated with Ekman pumping, even in early fall when the winds are strong and the pack-ice is weak, only has a small effect on the vertical heat transport. Furthermore, we estimate from the 1D heat budget a reduction of 1.4 m winter ice growth over three years (the residence time of ice in the Beaufort Gyre) associated with the missing Pacific Waters.

Abrégé

Ces dernières années, on a assisté à un recul important de la glace de mer dans le secteur Pacifique de l'Arctique. Une des causes possibles est l'augmentation du flux de chaleur océanique amplifié par la rétroaction glace-albédo. Cet article étudie le transport vertical de la chaleur de l'océan à partir des eaux d'origine pacifique et de la chaleur solaire dans la couche mixte et leur impact sur le bilan de masse de la glace de mer dans le Community Earth System Model - Large Ensemble (CESM-LE). À cette fin, nous nous concentrons sur deux périodes spécifiques avec des données hydrographiques d'observation provenant du Arctic Ice Dynamics Joint Experiment (1975-76) and des Ice-Tethered Profilers (2004-2018). Une comparaison entre les profils de salinité et de température potentielle simulés et observés met en évidence deux biais clés du modèle dans tous les membres de l'ensemble : une absence des eaux du Pacifique dans la colonne d'eau et un approfondissement de la couche mixte hivernale en opposition aux observations qui montrent une réduction de la profondeur de la couche mixte et une plus forte augmentation de la stratification. Les résultats d'un bilan thermique vertical unidimensionnel montrent que la chaleur solaire résiduelle piégée sous l'halocline est principalement ventilée vers la surface par le mixage vertical avant la saison de fonte suivante, tandis que l'advection verticale associée au pompage d'Ekman, même au début de l'automne lorsque les vents sont forts et que le pack-ice est faible, n'a qu'un faible effet sur le transport thermique vertical. En outre, nous estimons à partir du bilan thermique 1D une réduction de 1,4 m de la croissance de la glace d'hiver sur trois ans (le temps de résidence de la glace dans le mer de Beaufort) associée aux eaux manquantes du Pacifique.

Acknowledgements

Thank you Bruno Tremblay for your invaluable guidance and enthusiasm in science, writting and social involvement.

Thank you Erica Rosenblum for insightful comments and inspiring presence.

Thank you both for engaging meetings that always stimulated me to work even harder.

Thank you to the Sea Ice Group for still making me feel part of a community through this weird time.

Thank you to my partner Joe Lilek for always listening to me and providing comfort and/or solutions.

I would further like to thank FRQNT, NSERC, McGill University, Québec-Océan and Arctrain Canada for the opportunities and funding.Finally, I would like to acknowledge the CESM Large Ensemble Community Project and supercomputing resources provided by NSF/CISL/Yellowstone.

Table of Contents

List of Figures

List of Tables

Chapter 1

Forward

This Master's Thesis will be adapted to a paper that will be submitted to the Journal of Geophysical Research in the summer of 2021. All of the required elements for a thesis are included: an introduction with a comprehensive review of the relevant literature, a data & methodology section, research findings with a comprehensive scholarly discussion and a conclusion.

1.1 Manuscript Information

Title: Simulated and observed vertical hydrography in the Canada Basin: implications for vertical ocean heat transport under a transitioning sea ice cover
Authors: Juliette Lavoie, Bruno Tremblay and Erica Rosenblum
To be submitted to: Journal of Geophysical Research

1.2 Contributions of Co-authors

Juliette Lavoie, Bruno Tremblay and Erica Rosenblum collaborated on this project. Juliette Lavoie carried out the literature review as well as the experiments and analysis leading to the results. The writing was done in collaboration between Bruno Tremblay and Juliette Lavoie, with comments from Erica Rosenblum.

Chapter 2

Introduction

The Arctic has witnessed record retreat of sea ice extent (SIE) in recent years with the largest loss of ice in the Pacific sector (Beaufort and Chukchi Seas) [Fetterer, F. et al., 2017, McLaughlin et al., 2011]. This is unexpected because thick multiyear ice north of the Canadian Arctic Archipelago is being recicurlated in the Pacific Sector through the Beaufort Gyre – although, a more cyclonic ice circulation in the Canada Basin associated with a low bias in sea level pressure could explain some of the decline in the Pacific Sector [DeRepentigny et al., 2016]. Early signs of this Pacific-centric retreat were present even in 1997-98, when a thick multi-year ice floe, needed to set up the *Surface Heat Budget of the Arctic Ocean* (SHEBA) camp, proved difficult to find [Curry, 1999]. There is not yet a consensus for the cause of loss of multi-year ice in the Beaufort and Chukchi Seas. Possible causes include an increase in vertical heat flux in the Canada Basin (CB) [Carmack et al., 2015, Woodgate et al., 2010, Steele et al., 2010, Peterson et al., 2017, Maslowski et al., 2012], a trend in sea ice thickness from Arctic warming amplified by the ice-albedo feedback [Perovich et al., 2011a], a trend in coastal divergence in the Beaufort Sea [Kim et al., 2021], and increased ocean heat flux in the Bering Strait [Lenetsky et al., 2021]. While the observed Pacific-centric retreat of the pack ice is in agreement with 10 members of the Community Earth System Model-Large Ensemble (CESM-LE) and this model's predecessor the Community Climate System Model (CCSM) 4 [DeRepentigny et al., 2016, Desmarais and Tremblay, 2021], whether the model has the proper behavior for the correct reason remains unknown [Rosenblum and Eisenman, 2017]. The goal of this paper is to investigate the influence of vertical ocean heat flux on the sea ice mass balance in the CESM-LE during the transition from a perennial sea ice cover to a seasonal ice cover, and comparing the model to the hydrographic data from Arctic Ice Dynamics Joint EXperiment (AIDJEX) in 1975-76 and Ice-Tethered Profilers (ITP) data in 2004-2018 – two periods before and after the beginning of the transition to a seasonally ice free Arctic.

In an early study, the mean annual flux from the ocean to the ice was estimated at ~ 2 W m^{-2} from a 1D thermodynamic model constrained by observed surface radiative and turbulent fluxes from AIDJEX [Maykut and Untersteiner, 1971]. Later, Maykut and McPhee [1995] showed that the ice-ocean heat flux has a strong seasonality with a negligible winter mean and a summer mean of 40-60 W m^{-2}. The ice-ocean turbulent flux is dependant on the temperature of the mixed layer. Factors that can modify this temperature include strong winds events, resulting in fluxes as high as ~ 350 Wm^{-2} [Peterson et al., 2017], and changes in the bathymetry [Huwald et al., 2005]. A major driver of the mixed layer temperature is the input of shortwave flux to the ocean surface. Indeed, shortwave flux penetrating the ocean is correlated to bottom melt via the ice-ocean flux [Perovich et al., 2011b]. In recent years, the ice-ocean turbulent heat flux have increased substantially with more open water leading to a 4% per year increase in shortwave flux entering the ocean [Perovich et al., 2007]. Vertical ocean heat flux from depth into the mixed layer also influences the ice-ocean heat flux and the sea ice mass balance.

In the Canada Basin, there are three main sources of heat beneath the surface mixed layer: the Near Surface Temperature Maximum (NSTM), the summer/winter Pacific Waters (PW) and the Atlantic Waters (AW). The NSTM is remnant solar heat trapped beneath the mixed layer at the onset of ice formation [Maykut and McPhee, 1995, Perovich et al., 2008, Jackson et al., 2010, Steele et al., 2011]. Heat from the NSTM is ventilated during the fall and winter [Jackson et al., 2012] via convection associated with ice formation and brine rejection [Rudels et al., 1996, Timmermans, 2015] and enhanced turbulent mixing associated with inertial oscillations [Rainville et al., 2011]. Warm PW enters through the Bering Strait and are divided into three branches: (i) The Alaskan Coastal Current (ACC), which penetrates the Canada Basin, the Canadian Arctic Archipelago [Yamamoto-Kawai et al., 2008], Lancaster and Jones sounds [Jones et al., 2003] or continues along the coast on the Shelfbreak Jet [Pickart, 2004] where eddies break off the shelf and enters the Canada Basin [Manley and Hunkins, 1985, Pickart et al., 2005]; (ii) A second branch, which flows through the middle channel between Herald and Hanna Shoals and joins the ACC or flows over the shelf to the Canada Basin [Weingartner et al., 2005]; (iii) A third branch, which reaches Herald Canyon and flows over the shelf in the Canada Basin [Ladd et al., 2016, Gong and Pickart, 2015]. Warm and salty waters from the northern North Atlantic (AW) enter though the Fram Strait and the Barent Sea Opening, rejoin at the St Anna Trough and flow cyclonically around the Eurasian Basin into the Canada Basin [Nikolopoulos et al., 2009]. However, this layer does not meaningfully impact the sea ice mass balance as vertical heat fluxes through double staircase diffusion in the Atlantic Waters layer remain small (0.1 W m^{-2}) [Timmermans et al., 2008].

Heat moves vertically through the water column via diffusion or advection. Advection by Ekman transport in the Canada Basin has an impact on the vertical stratification and, therefore, on vertical heat fluxes. Indeed, Steele et al. [2011] argue that the downwelling of the Beaufort Gyre is partly responsible for the survival of the NSTM in that region as it is pushed below the mixed layer depth. The anticyclonic winds cause a convergence of surface ocean waters. In turn, this leads to downwelling in the center of the Canada Basin of the order $\sim$1 myr^{-1}, particularly in the fall when the winds are strong and the pack ice still weak [Proshutinsky et al., 2009, Meneghello et al., 2018b]. Ekman convergence is balanced by eddy diffusion [Davis et al., 2014]. Yet, Meneghello et al. [2018a, 2020] argue that the late winter thicker and slower ice cover drags the ocean acting as a governor, which removes the need for eddy diffusion to balance the gyre.

Diffusion moves heat from the NSTM and PW to the surface via small turbulence [Rudels et al., 1996], though the exact amount of diffusion is still debated [Shaw and Stanton, 2014, Jackson et al., 2012, Timmermans et al., 2008, Davis et al., 2016]. Errors in vertical mixing can lead to errors in heat leaving the ocean by up to 50 Wm^{-2} [Goosse et al., 1999] and also in simulation of the Atlantic and Pacific Waters flowing cyclonically or anticyclonically in the Canada Basin [Zhang and Steele, 2007]. In models, a proper representation of the halocline requires an accurate brine rejection parameterization as well as an accurate diffusivity with KPP parameterization [Nguyen et al., 2009, Large et al., 1994]. Though, most climate models still have difficulties simulating accurate stratification [Holloway et al., 2007, Ilıcak et al., 2016, Rosenblum et al., 2021a].

In the Arctic, the winter halocline is a permanent feature, sustained by lateral advection from the Eurasian shelf, as salt rejection from ice formation in the fall salinifies fresh shelf waters that find their level of equilibrium beneath the surface mixed layer [Aagaard et al., 1981]. The halocline separates the fresher and colder surface waters from the generally warmer and saltier deeper layers. The stratification also has a seasonal cycle [Lemke and Manley, 1984, Morison and Smith, 1981]: As ice melts in the summer, fresh water is released in the mixed layer creating a salinity profile with the seasonal halocline on top of the winter halocline [Rudels et al., 1996, Jackson et al., 2010]. In the fall, the seasonal halocline erodes, while brine rejection from ice formation increases the salinity of the mixed layer [Lemke and Manley, 1984]. Water temperature in the winter halocline can be near-freezing in the Eurasian Basin, referred to as the cold halocline layer, or cool in the Canada Basin where NSTM and PW are present beneath the mixed layer [Steele and

Boyd, 1998]. The strong gradient in salinity, together with the cold/cool halocline layer, creates a barrier that insulates the top of the ocean as salt rejection induced convection brings cold water to the surface, resulting in near zero vertical ocean heat flux. This contrasts the Southern Ocean where ice forms until the seasonal halocline is eroded [Aagaard et al., 1981, Rudels et al., 1996, Morison and Smith, 1981, Martinson, 1990].

Finally, the recent loss of ice in the Arctic is driving two competing mechanisms affecting the vertical heat transport: (1) reduced vertical mixing due to surface freshening and increased stratification, and (2) increased vertical mixing due to a thinner and more mobile pack ice. Hydrographic observations in the Canada Basin in recent decades clearly show a reduction of the mixed layer pointing to the dominance of increased stratification [Peralta-Ferriz and Woodgate, 2015]. Whether these processes are well-represented in global climate models is crucial to understanding the evolution of the ice-ocean heat flux and sea ice mass balance.

Auclair and Tremblay [2018] found a link between ocean heat transport through the Bering Strait and rapid sea ice decline on the continental shelf in the CESM-LE. When the pack ice migrates northward over the deep ocean, rapid declines are caused instead by anomalies in radiative fluxes and ice transport. The goal of this paper is to assess the accuracy of the simulated vertical ocean heat flux in the retreat seen during the transition from a seasonal to a perennial ice cover over the deep basin. To this end, the simulation of the CESM-LE is analyzed compared to observations to assess the biases of the model [Holloway et al., 2007, Ilıcak et al., 2016, Rosenblum et al., 2021a].

The structure is as follows. Chapter 3 presents the observations (3.1.1), the model (3.1.2)) and the methods (3.2). Chapter 4 presents the results and discussion and is divided in three parts: (4.1) the bulk heat budget of the ice-ocean system, (4.2) the simulated and observed vertical profiles in the surface ocean and (4.3) a 1D vertical heat transport budget. Chapter 5 presents a conclusion and summary of the results.

Chapter 3

Data and Methods

3.1 Data

3.1.1 Observations: AIDJEX and ITP

We use Canada Basin temperature and salinity profiles from the AIDJEX [Moritz, Richard, 2020] and ITP [Krishfield et al., 2008], which were collected during 1975 - 1976 and 2004 - 2018, respectively (Figure 3.1). Profiles with data between 10 m - 490 m – range common to most profiles – were interpolated on a 1m resolution grid. AIDJEX consisted of four ice camps deployed between $75-78°$N and $143-148°$ W in April 1975 that drifted southwest in the Beaufort Sea. ITP buoys selected for analysis cover the full Canada Basin ($72-80°$N and 130-155 °W). 36 ITPs were deployed in the period 2004-2018, taking measurements once or twice a day, each with an average life span of 260 days consisting of 15303 profiles. There is a large difference in the number of data points between AIDJEX and ITP. However, the differences between the periods highlighted in this paper by looking at averages remain true for a majority of profiles.

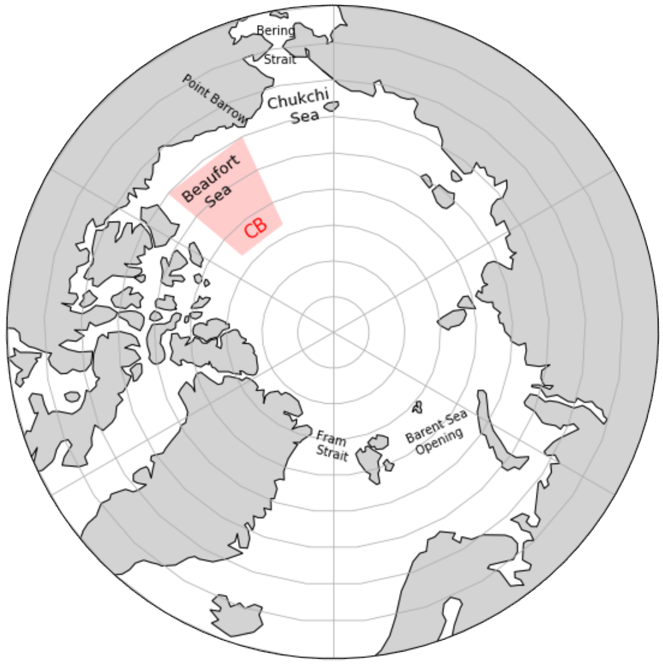

Figure 3.1: Arctic domain and definition of the Canada Basin ($72-80$°N and 130-155 °W). The blue dots are located at the center of each grid cell within the Basin in the native CESM grid.

3.1.2 Model: CESM-LE

The Community Earth System Model (CESM1) has four components. The sea ice component is the Community Ice CodE (CICE 4), which has four ice layers and one snow layer. It includes a subgrid-scale ice thickness distribution (ITD) [Bitz et al., 2001, Lipscomb, 2001], an energy conserving thermodynamics scheme that accounts for brine pockets [Bitz and Lipscomb, 1999] and an elastic-viscous-plastic rheology [Hunke and Dukowicz, 1997]. The ITD has five ice categories: 0 m - 0.64 m - 1.39 m - 2.47 m - 4.57 m - ∞. The ocean component is the Parallel Ocean Project (POP 2), which has 60 vertical layers with a vertical resolution ranging from 10 m to 250 m at depth. It uses the K-profile parameterization (KPP) vertical mixing parameterization [Large et al., 1994], the Gent-McWilliams parameterization for horizontal tracer diffusion [Gent and Mcwilliams, 1990], anisotropic horizontal viscosity [Large et al., 2001], and third-order upwind advection for tracers [Leonard, 1979]. The freezing temperature is fixed at -1.8°C. The land component is the Community Land Model (CLM 4), which uses the SIMTOP scheme for drainage and sub-surface runoff [Niu et al., 2005]. The atmosphere component is the Community Atmosphere Model (CAM 5), which has 30 layers and uses the Rapid Radiative Transfer Method [Iacono et al., 2008, Mlawer et al., 1997]. All components have a nominal spatial resolution of 1°, resulting in an effective resolution of 40-70km in the Arctic. The pole of the ocean and ice grid is located over Greenland, in order to avoid the singularity at the pole. The Arakawa B-grid is used with tracers defined at the grid center and vectors defined on the vertices.

The CESM - Large Ensemble (CESM-LE) is a set of 40 ensemble members (EMs) - based on the CESM1 – differing only by a slightly varying initial conditions [Kay et al., 2015]. The model was initialized using observed ocean temperature and salinity, as well as, atmosphere, land and sea ice conditions from an existing CESM1 run. It ran under constant pre-industrial forcing for 1500 years until the model reached equilibrium. The first ensemble member (EM1) was initialized from a random date of the constant 1850 forcing period and run for an additional 250 years. Other EMs were initialized with 1920 EM1 values and with a one day lag in ocean conditions (EM2) or a given random perturbations of the order of 10^{-14}K in the air temperatures (EM3-40). All EMs are run with observed CO_2 concentration from initialization to 2005 and with RCP8.5 from 2006 to 2100.

3.2 Methods

In section 4.2, the CESM-LE and ITP profiles are averaged over grid cell with SIC $> 60\%$ as the observations are biased toward cooler temperatures. When the ITP is in a zone of low ice concentration, it is biased towards cold temperature as it is attached below to a thicker floe. Hence, we compare model and observations for higher SIC (see Figure 3.2).

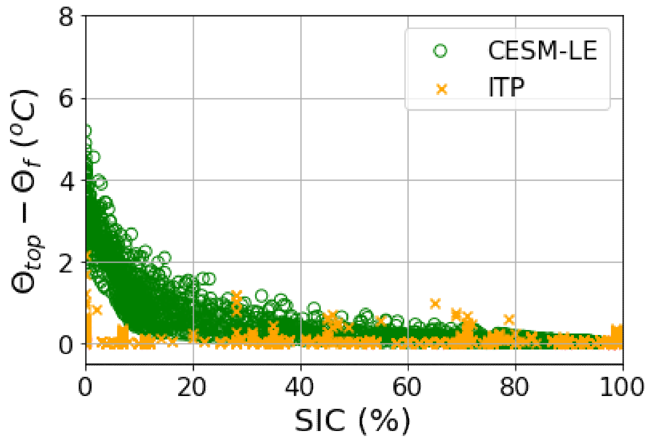

Figure 3.2: September top (valid value closest to the surface) temperature away from freezing vs. sea ice concentration (SIC) over the Canada Basin for ITP (yellow crosses) and the CESM-LE (green circles) (showing only one ensemble member as an example for clarity).

Next, the conservation energy equation is used to calculate a 1D (vertical) ocean heat budget over the top 200m.

$$\rho\frac{\partial e}{\partial t} + \rho w\frac{\partial e}{\partial z} = D + R, \tag{3.1}$$

where e ($= c_p\Theta$) is the internal energy per mass unit (J kg^{-1}), c_p is specific heat of sea water (J kg^{-1} °C^{-1}), Θ is the potential temperature (°C^{-1}), ρ is the density (kg m^{-3}), w is the vertical velocity (m s^{-1}), D is the vertical diffusion of heat (J s^{-1} m^{-3}), and R is the divergence of surface radiative fluxes (J s^{-1} m^{-3}).

The energy equation can be written in flux form using the continuity equation:

$$\frac{\partial \rho}{\partial t} + w\frac{\partial \rho}{\partial z} + \rho\frac{\partial w}{\partial z} = 0. \tag{3.2}$$

Multiplying eq. 3.2 by e and adding it to eq. 3.1 gives:

$$\frac{\partial E}{\partial t} = R + D - \frac{\partial (wE)}{\partial z}, \tag{3.3}$$

where $E = e\rho$ is the internal energy per volume unit (J m^{-3}). These four terms will be calculated from CESM-LE output as defined below. The 40 ensemble members are used to estimate the uncertainty in each term associated with natural variability.

The tendency for the internal energy is calculated using a second order centered finite difference scheme as

$$\left.\frac{\partial E}{\partial t}\right|_t = \frac{E_{t+1} - E_{t-1}}{2\Delta t}, \tag{3.4}$$

where $E(t)$ is monthly mean temperature for month t and Δt is the difference between two time steps (1 month). We use the monthly mean temperature because snapshots in the CESM-LE simulation are only stored every 5 years. This will lead to an error of $O(\Delta t^2)$ that will be discussed below in section 4.1.

The simulated divergence of surface fluxes (R) is given by

$$R = \begin{cases} \frac{\partial}{\partial z}\left(F_{sw,ao} + F_{sw,io} + F_{lw} + F_{sens} + F_{evap} + F_{frazil}\right), & \text{if } z = z_1 \\ \frac{\partial}{\partial z}\left(F_{sw,ao} + F_{sw,io}\right), & \text{otherwise,} \end{cases} \tag{3.5}$$

where z_1 is first layer at the top of the water column, $F_{sw} = F_{sw,ao} + F_{sw,io}$ is the shortwave flux (W m^{-2}), which penetrates the ocean directly from the atmosphere to the ocean (ao) and from the atmosphere through ice to the ocean (io), F_{lw} is the longwave flux (atmosphere/ocean), F_{sens} is the sensible heat flux (atmosphere/ocean), F_{evap} the latent heat flux from evaporation or deposition (atmosphere/ocean), and F_{frazil} is the latent heat from the formation of new ice in the ocean over open water, i.e. the heat required to warm the supercooled water ($\Theta < -1.8$°C) to freezing point temperature and is calculated as an equivalent downward heat flux by the CESM-LE. The simulated shortwave flux decays exponentially with depth following Beer's Law and chlorophyll levels, based on Ohlmann [2003]. The longwave, sensible, evaporation, and frazil fluxes do not penetrate below the first layer, implying that $\frac{\partial F}{\partial z} = \frac{\Delta F}{\Delta z} = \frac{F}{\Delta z}$, where Δz is the thickness of the layer. Heat fluxes that lead to an increase in the ocean temperature are taken to be positive.

The simulated vertical diffusion of heat (D) is given by

$$D = \begin{cases} D_{VM} + D_{iso} + \frac{F_{io}}{\Delta z}, & \text{if } z = z_1. \\ D_{VM} + D_{iso}, & \text{otherwise,} \end{cases} \tag{3.6}$$

where D_{VM} is the vertical mixing from the KPP parameterization, D_{iso} is the vertical component of isopycnal mixing from the Gent-McWilliams parameterization, and F_{io} is the ice-ocean turbulent heat flux (which depends on the gradient of temperature between the ice base and the mixed layer, similar to D_{VM}),

$$F_{io} = \rho c_p c_h u_* (\Theta - \Theta_f), \tag{3.7}$$

where c_h is a heat transfer coefficient and u_* is the friction velocity.
D_{VM} is composed of a diabatic (D_{dia}) and a non-local term, (D_{nl})

$$D_{VM} = D_{dia} + D_{nl} = c_p \rho \left[\frac{\partial}{\partial z}(\kappa \frac{\partial \Theta}{\partial z}) - \frac{\partial}{\partial z}(\kappa \gamma_{_\Theta}) \right], \tag{3.8}$$

where κ is the diffusivity and $\gamma_{_\Theta}$ is the non-local vertical heat flux, which represents mixing associated with convection and unstable vertical stratification.

The error in the 1D heat budget is calculated from the residual, which includes non-resolved horizontal advection and diffusion as well as the error ($O(\Delta t^2)$) from the second order finite difference approximation of the time derivative.

Following Peralta-Ferriz and Woodgate [2015], the mixed layer depth (MLD) is calculated as the shallowest depth where the change in potential density ($\Delta\sigma$) is larger or equal to the 0.1 kg m^{-3} threshold.

$$\Delta\sigma = \sigma(z) - \sigma(z_{min}) \geq 0.1kgm^{-3}, \tag{3.9}$$

where z_min is the shallowest measured depth.

The correspondence between the names of variables in this paper and their name in the CESM-LE is shown in the appendix (Table 6.1).

Chapter 4

Results and Discussion

4.1 Heat Budget

To first order, the mean July 1970-1979 ice-ocean heat budget is a balance between the net solar radiation ($F_{sw,ao} = 29.77 \pm 2.98$ W m^{-2}), turbulent ice-ocean heat flux ($F_{io} = -22.74 \pm 1.94$ W m^{-2}), and the change in internal energy of the entire water column ($\frac{\partial E}{\partial t} = 9.22 \pm 1.76$ W m^{-2} – see figure 4.1). The sea ice mass balance is mainly controlled by thermodynamic effects, with a small contribution from ice export of -3.73 ± 7.25 cm averaged over the summer. Integrated over the summer, the basal sea ice melt (60.11 ± 7.14 cm), which is associated with the turbulent ice-ocean heat flux and a negligible contribution from the conductive heat flux, is larger than the surface melt (33.78 ± 5.82 cm; not shown). This is in general agreement with observations from AIDJEX [34 cm vs 26 cm for basal and surface melt respectively, Maykut and McPhee, 1995]. However, the model differs from some earlier measurements made in the 1950s that have very large variabilty. For example, Untersteiner [1961] reports basal and surface melt of 22 cm vs 19 cm and 24 cm vs 41 cm in 1957 and 1958 from measurements made in the same region as part of the US Drifting Station A of the International Geophysical Year.

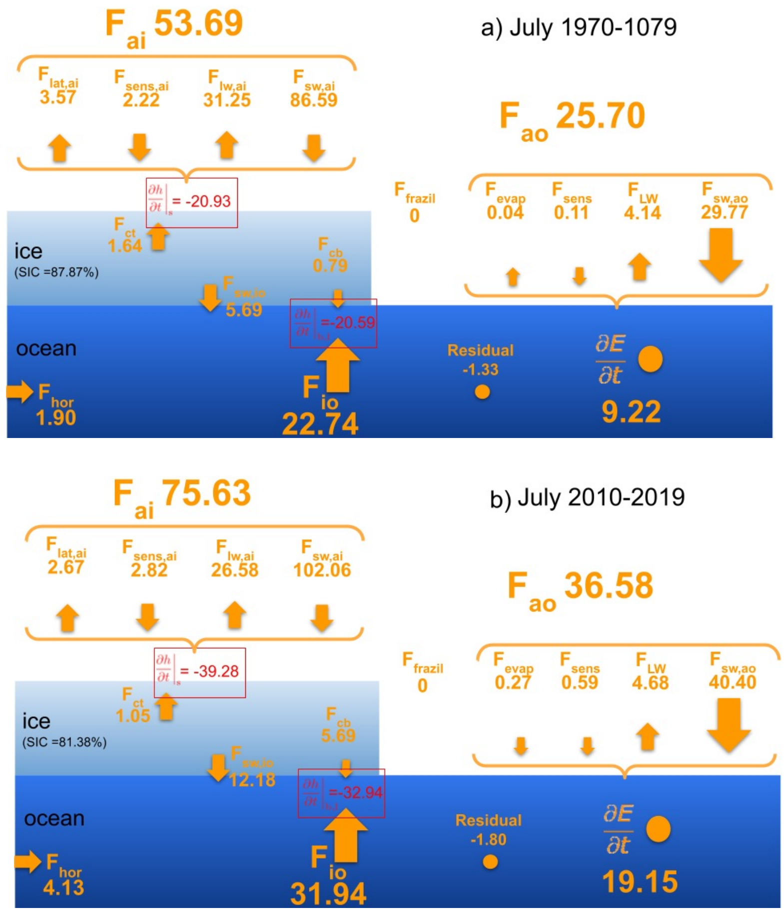

Figure 4.1: CESM-LE ensemble-mean ice-ocean heat budget for July averaged spatially over the Canada Basin and temporally over the years a) 1970-1979 or b) 2010-2019. Changes in ice thickness $\frac{\partial h}{\partial t}$ (red) are expressed in cm/day and all fluxes F (orange) are expressed in Wm^{-2}. F_{hor} is the sum of vertically-integrated temperature tendencies from horizontal diffusion and advection. F_{cb} and F_{ct} are the conduction fluxes at the bottom and the top of the ice. All other variable names are defined in section 3.2.

The second order terms in the July heat budget include solar flux transmitted through the ice ($F_{sw,io} = 5.69 \pm 0.94$ W m^{-2}), longwave cooling over open ocean ($F_{lw} = -4.14 \pm 0.56$ W m^{-2}), and lateral ocean heat transport ($F_{hor} = 1.90 \pm 0.79$ W m^{-2}). The main contribution of the lateral ocean heat transport is advection by the mean flow and eddies; the advection by sub-mesoscale eddies is negligible (results not shown). When considering all terms, the heat budget closes to within -1.33 ± 0.52 W m^{-2}, which is approximately 5% of the first order terms (F_{io} and $F_{sw,ao}$). This error mainly comes from the second order finite difference approximation of the internal energy tendency term ($\frac{\partial E}{\partial t}$) using the monthly mean ocean temperatures as opposed to instanteneous temperatures.

We find numerous differences between the July ice-ocean surface heat budget in 1970-1979 and 2010-2019. First, both the solar heat flux into the ocean and the ice-ocean turbulent heat flux is 40% larger in 2010-2019 than in 1970-1979. Second, the transmitted shortwave radiation through the snow/ice and the internal energy of the ocean both doubled. The larger transmitted shortwave radiation through the ice in 2010-2019 is due to reduced snow depth and ice thickness. The large increase in internal energy is due to a bias low in ice-ocean turbulent heat flux despite a large warming of the surface ocean and the absence of an increased in stratification with increased sea ice melt (see discussion in Section 4.2). The basal and surface melt in the CESM-LE in the early 2000s (start of the transition to a seasonally ice free Arctic) are in general agreement with observations from post-2000 Ice Mass Balance buoys in the Beaufort Sea [97.64 ± 7.95 cm vs 61.92 ± 6.73 cm in the CESM-LE and 106 cm vs 62 cm in observations, Perovich and Richter-Menge, 2015]. Changes in sea ice volume due to dynamical process (-1.96 ± 7.09 cm) are again negligible compared to thermodynamic processes.

In February, the first order balance in the 1970-1979 ice-ocean heat budget is between the latent heat associated with freezing (18.15 ± 1.12 W m^{-2}, or 14.35 ± 0.88 cm of ice growth) and the conductive heat flux at the bottom of the ice ($F_{cb} = -18.30 \pm 1.10$ W m^{-2}). The small difference between latent and conductive heat flux is indicative of the small contribution from turbulent ice-ocean heat flux. The thermodynamic and dynamic ice growth, integrated over the full winter is equal to 35 ± 9 cm in the 2.47 – 4.57 m ice thickness category (or 115.21 ± 5.46 cm in all thickness categories) is in agreement with observations of 57 cm [including only the thermodynamic tendency, Untersteiner, 1961]. The ice growth in the second thickest ice category is used in accord with mean ice thickness measurements in the Canada Basin. Looking at thinner ice would be biased to faster growth compared to thick ice floes where instruments are installed.

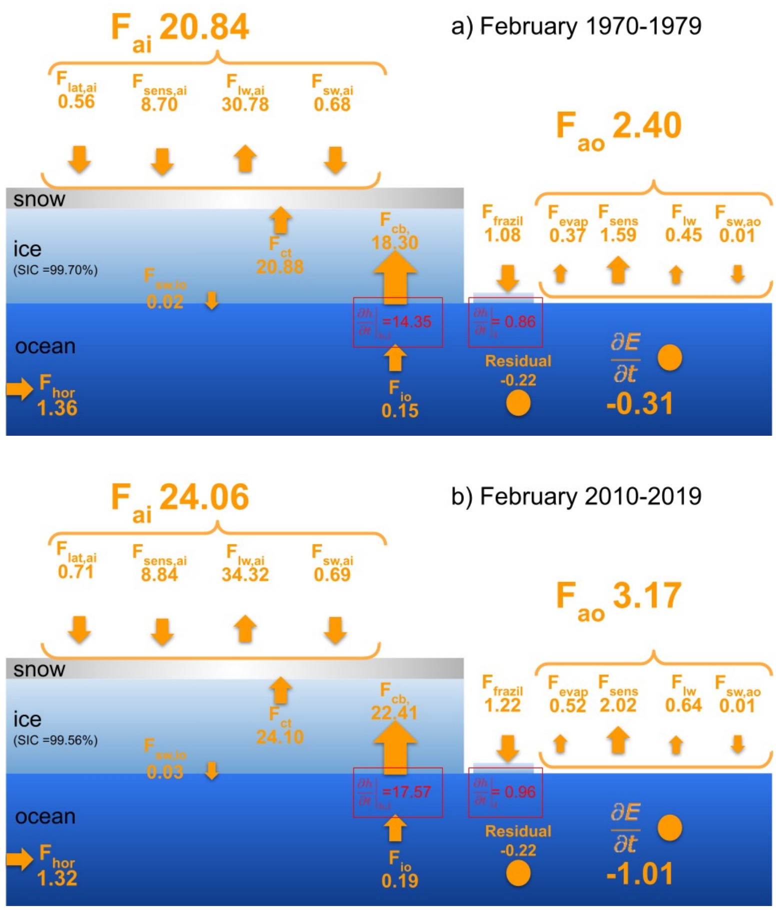

Figure 4.2: CESM-LE ensemble monthly mean heat budget for February averaged spatially over the Canada Basin and temporally over the years a) 1970-1979 and b) 2010-2019. Change in ice thickness $\frac{\partial h}{\partial t}$ (red) are expressed in cm/day. All fluxes F (orange) are expressed in Wm^{-2}. F_{hor} is the sum of vertically-integrated temperature tendencies from horizontal diffusion and advection. F_{cb} and F_{ct} are the conduction fluxes at the bottom and the top of the ice. All other variable names are defined in section 3.2.

The second order balance in February heat budget is between the ice-atmosphere sensible heat flux through the leads ($F_{sens} = -1.59 \pm 0.16\ Wm^{-2}$), the latent heat flux associated with frazil ice formation ($F_{frazil} = 1.08 \pm 0.12\ Wm^{-2}$), lateral ocean heat transport ($F_{hor} = 1.36 \pm 0.63\ Wm^{-2}$), and change in internal energy ($\frac{\partial E}{\partial t} = -0.31 \pm 0.46\ Wm^{-2}$). Each term is nearly of the same order of magnitude as the residual error in the net heat budget

$(-0.22 \pm 0.52 W m^{-2})$.

Between 1970-1979 and 2010-2019 time periods, the basal growth is larger by 20% due to a decrease in ice/snow thickness and despite the reduced temperature gradient between the surface and ice base (ie. the negative ice growth-ice thickness feedback). However, the increased growth in the winter does not compensate for the 60% (87%) increase in basal (surface) melt. In the 2010-2019 time period, the ice growth integrated over the winter for the 2.47 – 4.57 m thickness category is equal to 57 ± 13 cm (or 136.29 ± 7.92 cm over all ice thickness categories) is in accord observations [59 cm, Perovich, D. et al., 2021]. At the same time, the horizontal flux and the ice-ocean turbulent flux stayed nearly constant .

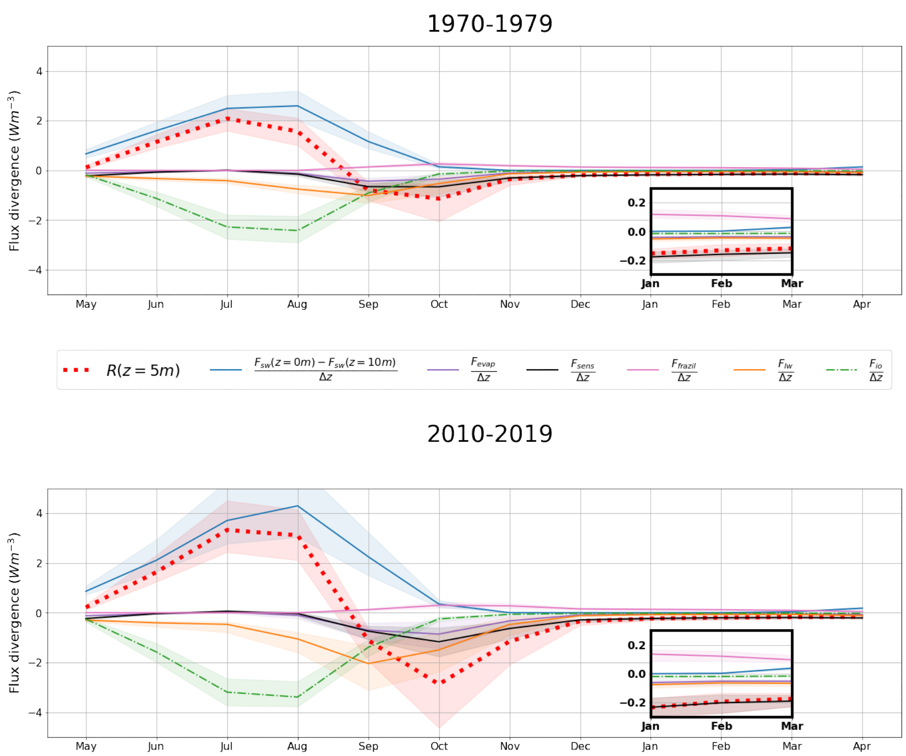

Figure 4.3: Simulated monthly divergence of fluxes in the top layer of the ocean in (top) 1970-1979 and (bottom) 2010-2019. The figure shows the divergence of the turbulent ice-ocean flux (part of D) and all the components of R in the top layer (at $z = z_1 = 5$ m) (see eq. 3.5). The shaded region represents the basin-average maximum/minimum over the 40 ensemble members.

The fluxes calculated in this bulk ice-ocean budget will be used in the first layer of R (see eq. 3.5) in the 1D vertical heat budget. Figure 4.3 shows the complete seasonality of surface flux. The summer is dominated by the shortwave flux. In the fall, the heat is mostly leaving the surface by sensible and longwave flux over open water. In the winter, the most important flux is the sensible flux over leads, while the ice-ocean turbulent flux remains small. Hence, the heat stored in the ocean and ventilated in the winter is mostly use to impede the growth of new ice in leads rather than basal growth of exsiting ice.

4.2 Vertical T-S Profiles: CESM-LE vs Observations

Heat in the Canada Basin comes from three different sources located at different depths: the Near Surface Temperature Maximum (NSTM), the Pacific Waters (PW), and the Atlantic Waters (AW) (see figure 4.4).

From the 1970s to the early 2000s, observations indicate that the three September temperature maxima (NSTM, PW, AW) in the Canada Basin warmed by 0.09°C, 0.22°C, and 0.39°C, respectively (see Figure 4.4a). The surface ocean also became more stably stratified, with a reduction in the mixed-layer depth of 8 m and a reduction of sea surface salinity of 2.3 psu, as in [Rosenblum et al., 2021b]. We also find that the winter PW (the second bump in the PW shaded area) is more visible in the early 2000s than in the mid-1970s; Whether this is due to sampling or warming is not clear.

By contrast, the CESM-LE shows very little change between 1970-1979 and 2010-2019 (Figure 4.4b). The temperature is nearly unchanged over the top 400 m, with the NSTM only warming by 0.06 °C. Similarly, the stratification is nearly the same, with only a 0.6

psu average change in salinity over the top 400 m, as in [Rosenblum et al., 2021a].

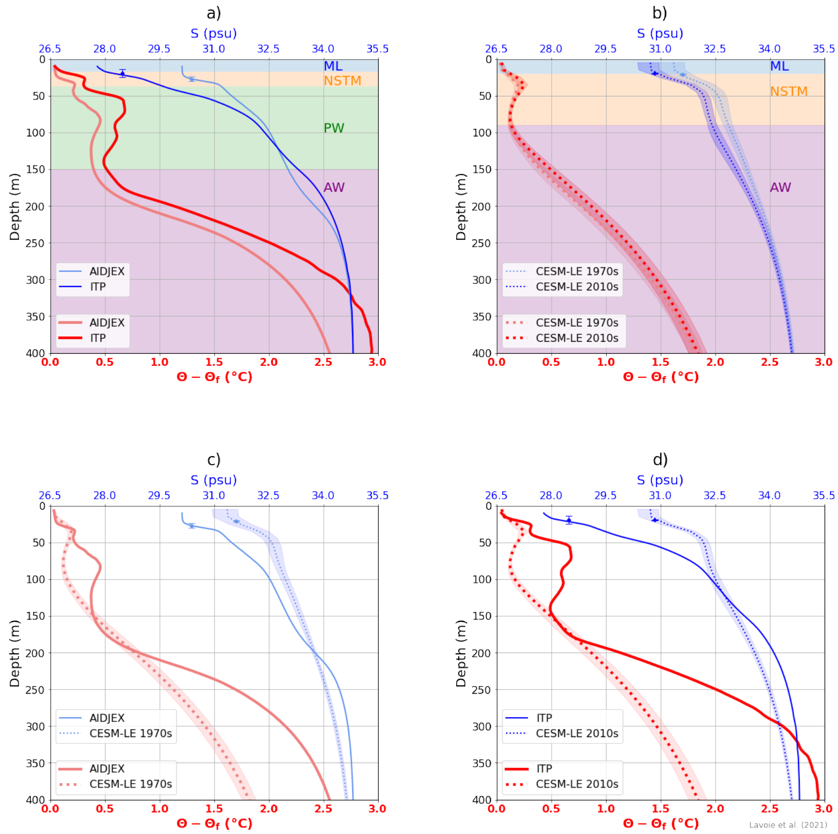

Figure 4.4: Observed and simulated September potential temperature anomaly from freezing (blue) and salinity (red) averaged over the Canada Basin in 1970-1979 and 2010-2019. a) Observations from 1975-76 (AIDJEX) and 2004-2018 (ITP), b) CESM-LE ensemble mean from 1970-1979 and 2010-2019, c) AIDJEX and CESM-LE 1970-1979, d) ITP and CESM-LE 2010-2019. (a,b) The Mixed Layer (ML), Near-Surface Temperature Maximum (NSTM), Pacific Water (PW), and Atlantic Water (AW) are indicated by blue, yellow, green, and purple shadings, respectively. The diamonds and error bars indicate the averaged mixed layer depths and standard deviations. The shaded region represents the maximum/minimum basin-average over the 40 ensemble members.

Perhaps the most striking difference between the model and the observations is the complete absence of PW in the CESM-LE between 50 m and 100 m (see figure 4.4 c and d). This bias is likely related to an unrealistic PW pathway through through the Arctic, as in CCSM3 (an earlier version of the CESM-LE) [Jahn et al., 2010]. Specifically, they found that the eastern PW branch does not penetrate far east and instead is entrained in a clockwise direction following the surface Beaufort Gyre around Point Barrow. The CESM

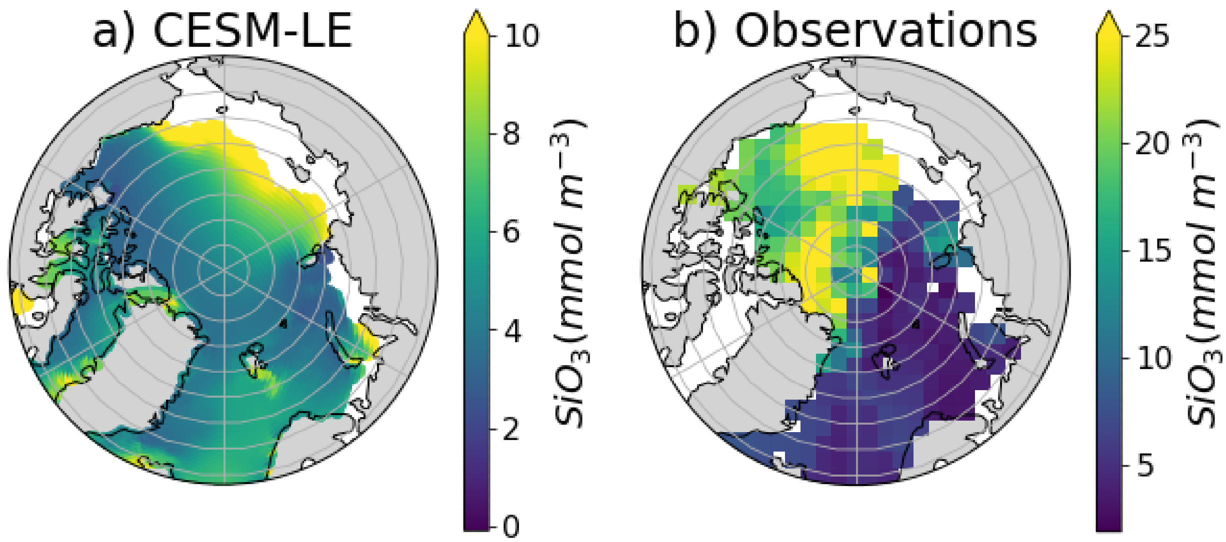

Figure 4.5: (a) Simulated and (b) observed summer (JAS) mean dissolved inorganic silicate average at 75m depth between 1948 and 2000 using the CESM ensemble mean and observations come from the World Ocean Atlas [Boyer et al., 2018]. White space represents the shelf, which is shallower than 75m.

probably has similar pathways as its predecessor since CCSM3 dye tracer results are in accord with the spacial distribution of silicate - a tracer used to track PW simulated by the CESM-LE (see figure 4.5). In-situ observation of silicates instead suggests that there is a large amount of PW in the Canada Basin entering directly from the Bering Strait over the Chukchi sea sea or via eddies breaking off the Alaskan Coastal Current [Pickart et al., 2005, Weingartner et al., 2005, Ladd et al., 2016].

Overall, the observed transition to a warmer more stratified Canada Basin from the 1970s to the early 2000s is missing in the CESM-LE. In the observations, there is a large freshening of the surface water for all months and a clear reduction of the May MLD (Figure 4.6 a and c; as in Peralta-Ferriz and Woodgate [2015], Rosenblum et al. [2021b]). Yet, in the CESM-LE, there is only a small freshening of the surface water and the winter mixed layer thickens instead (see figure 4.6 b and d). We note that the May MLD is well-represented in the CESM-LE in the 1970s, but fails to respond to the freshwater flux associated with sea ice thinning in the early 2000s (see figure 4.7). These findings are consistent with Rosenblum et al. [2021a], who show that the model bias can be partly attributed to unrealistic vertical mixing, rather than sea ice melt. It appears that the net effect of increased melt and surface mixing by surface stress causes a more stable stratification in the observations and a less stable stratification in the CESM-LE. That is, the competition between wind-driven surface stress and fresh water input created by the recent large ice melting is won by fresh water input with increased stratification in observations [Peralta-Ferriz and Woodgate, 2015], and by increased surface stress in the CESM-LE. This difference in stratification will have a large impact on vertical mixing between the mixed layer and the heat at depth [Toole et al., 2010].

The reduction of the mixed layer depth has repercussions on the ventilation of the NSTM. In 1975-1976 (AIDJEX), the observations indicate that the NSTM is only completely ventilated in May (see figure 4.6a). In 2004-2018, the observations (ITP) indicate that the NSTM has disappeared by December (Figure 4.6c). Whether it was ventilated to the surface or it merged with summer PW just beneath remains unclear. When looking at individual profiles, there is large spatial and/or time variability: In the 1970s, the NSTM is absent from spring 1975, but clearly present in spring 1976 for the Caribou and BlueFox camps (see figure 4.8). This is presumably due to the fact that the camps started far north (high SIC) and drifted south (low SIC), where the open waters create better conditions for the creation of a warm NSTM. In the 2000s, the NSTM disappears between January (or earlier) and April (see ITP 41,75,53,82 in figure 4.9). Despite the large spatial/temporal variability, the NSTM in ITP data is less well-defined in the fall/winter and is ventilated more quickly than in AIDJEX presumably due to the more mobile thinner pack ice in the fall. In the CESM-LE, the ventilation of the NSTM lasts until May in both the 1970s and the 2000s, again missing a key transformation between the two time periods (figure 4.6b and d).

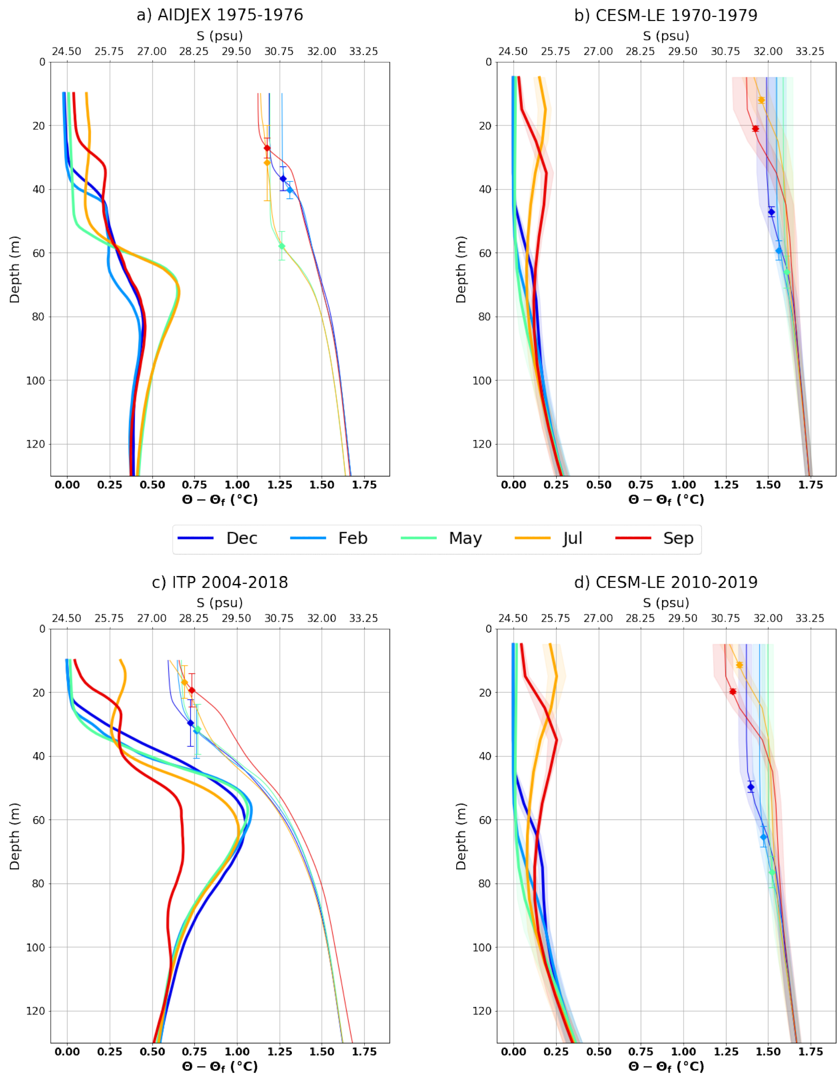

Figure 4.6: Observed and simulated monthly-mean, basin-average profiles of potential temperature anomaly from freezing (thick lines on the left) and salinity (thin lines on the right) using observations from (a) 1975-76 (AIDJEX) and (c) 2004-2018 (ITP), and the CESM-LE ensemble mean averaged over (b) 1970-1979 and (d) 2010-2019. The diamonds and error bars indicate the averaged mixed layer depth and the standard deviation. The shaded region indicates the basin-average maximum/minimum over the 40 ensemble members.

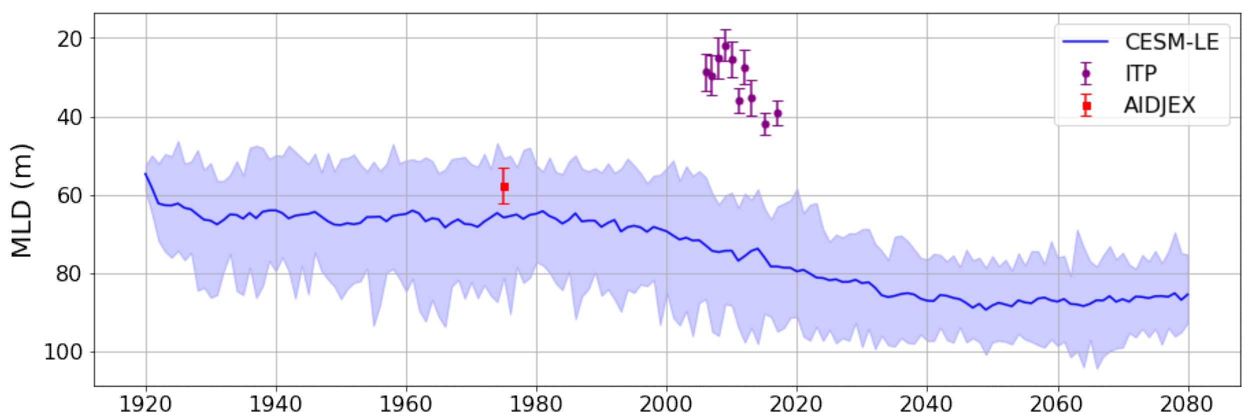

Figure 4.7: Observed and simulated May mixed layer depth (MLD) averaged over the Canada Basin between 1920 to 2080. The solid line indicates the ensemble mean and the shaded region indicates the basin-average minimum/maximum range over the 40 ensemble members. The purple round/red square markers indicate the observed mean and standard deviation of mixed layer depth from 1975-76 (AIDJEX) and 2004-2018 (ITP).

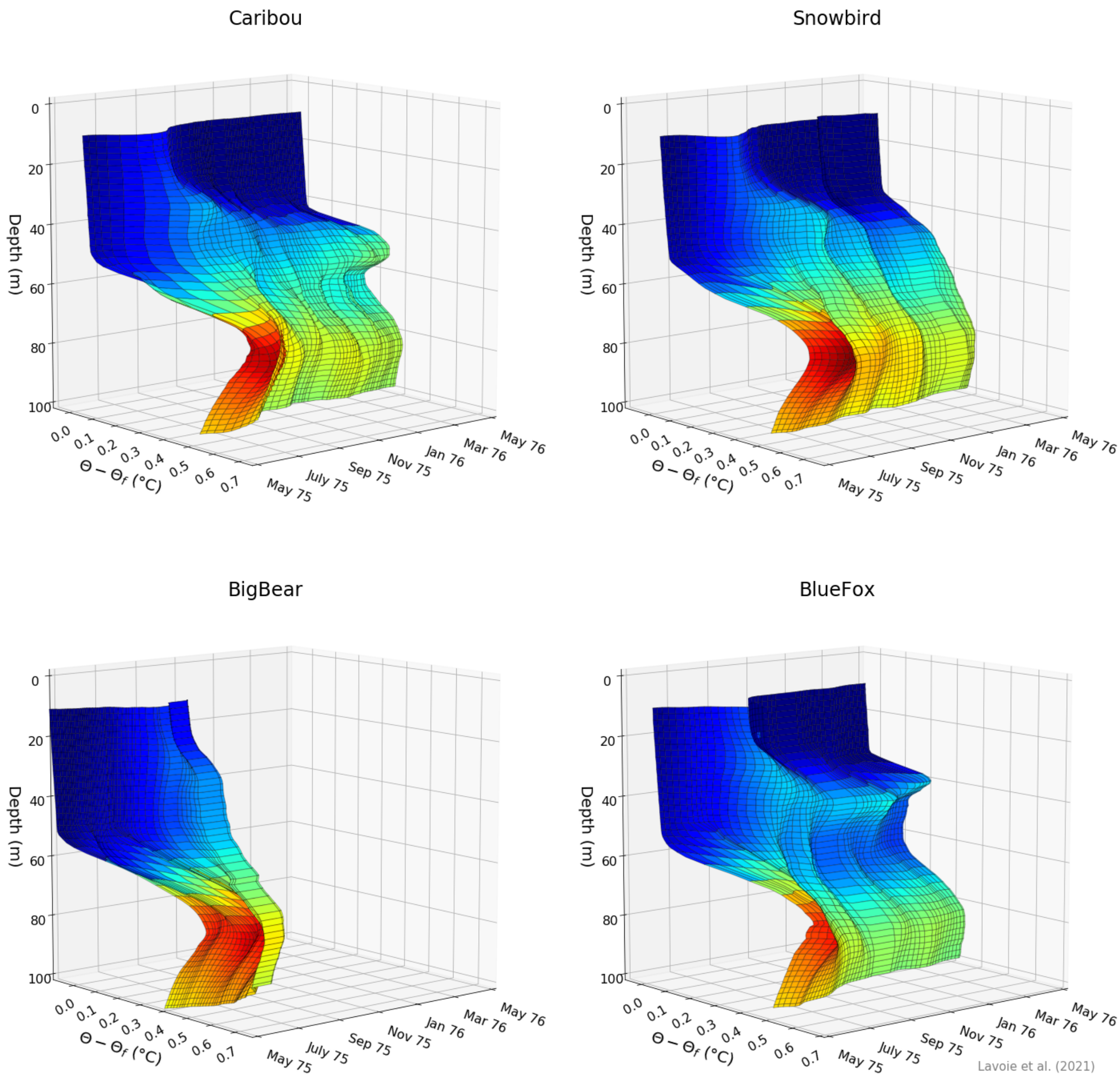

Figure 4.8: Observed seasonal evolution of the potential temperature anomaly from freezing profiles for the four 1975-1976 AIDJEX camps. The profiles have been smoothed in time with a Gaussian filter. Figure inspired by Maykut and McPhee [1995].

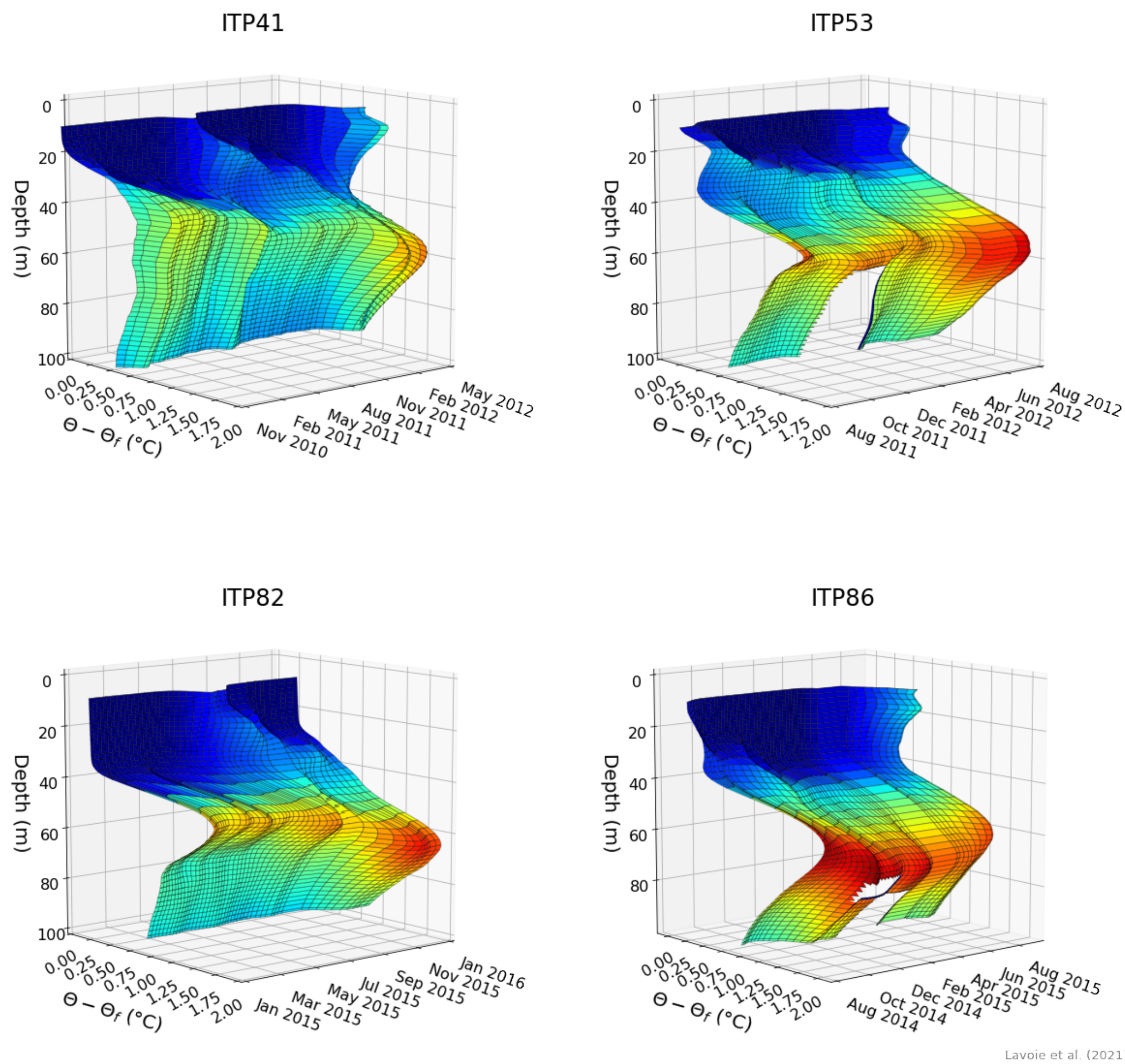

Figure 4.9: Observed seasonal evolution of the potential temperature anomaly from freezing profiles for four representatives (out of 36) ITPs. The profiles have been smoothed in time with a Gaussian filter. Note that the time axis is different for each subplot. Figure inspired by Maykut and McPhee [1995].

4.3 1D Heat Budget: Vertical Transport

We examine the CESM-LE basin-average change of heat at each depth ($\frac{\partial E}{\partial t}$) in response to three processes (equation 3.3): divergence of surface fluxes R, vertical diffusion D, and vertical advection $-\frac{\partial (Ew)}{\partial z}$ (see figure 4.10). In the following, the focus is on the 2000s when the same processes are observed and are more apparent than in the 1970s.

In the summer, the main balance is between the divergence of the surface fluxes (R), dominated by the shorthwave flux, and the turbulent mixing (D), with the change in internal energy as a second order term ($\frac{\partial E}{\partial t}$). In early summer, the SIC is high and surface fluxes entering the mixed layer leads to ice melt via ice-ocean turbulent at flux. Less importantly, heat from the NSTM is diffused upward to the surface by diffusion.

In the fall, this balance reverses and heat stored below the surface ($\frac{\partial E}{\partial t}$) is brought up to the surface by diffusion (D) and lost to the atmosphere by surface fluxes (R), mostly sensible and longwave. In late summer and early fall, the change in internal energy are large as the sea ice concentration is much lower. At depth, some heat is gained through penetrating shortwave (R) until about 40 m.

From November to April, the heat stored in the NSTM is ventilated – matching negative peaks in $\frac{\partial E}{\partial t}$ and D that decreases in amplitude and increases in depth – with convection induced by salt rejection that erodes the seasonal halocline and deepens the mixed layer. The heat brought up by diffusion leaves the ocean through surface fluxes (R), mainly with the sensible flux through leads. There is no solar flux in winter, hence there is no surface flux below the first layer of the ocean.

Vertical heat flux associated with Ekman pumping downward (1 to 20 myr^{-1}) is highest in the fall when the winds are strong and the pack still relatively open and weak [Meneghello et al., 2018b, Petty et al., 2016], but even then, is relatively small compared with other terms in the budget. The near zero advection term in the winter is consistent with the weakening of the anticylonic ice drift associated with thick ice [Meneghello et al., 2018b].

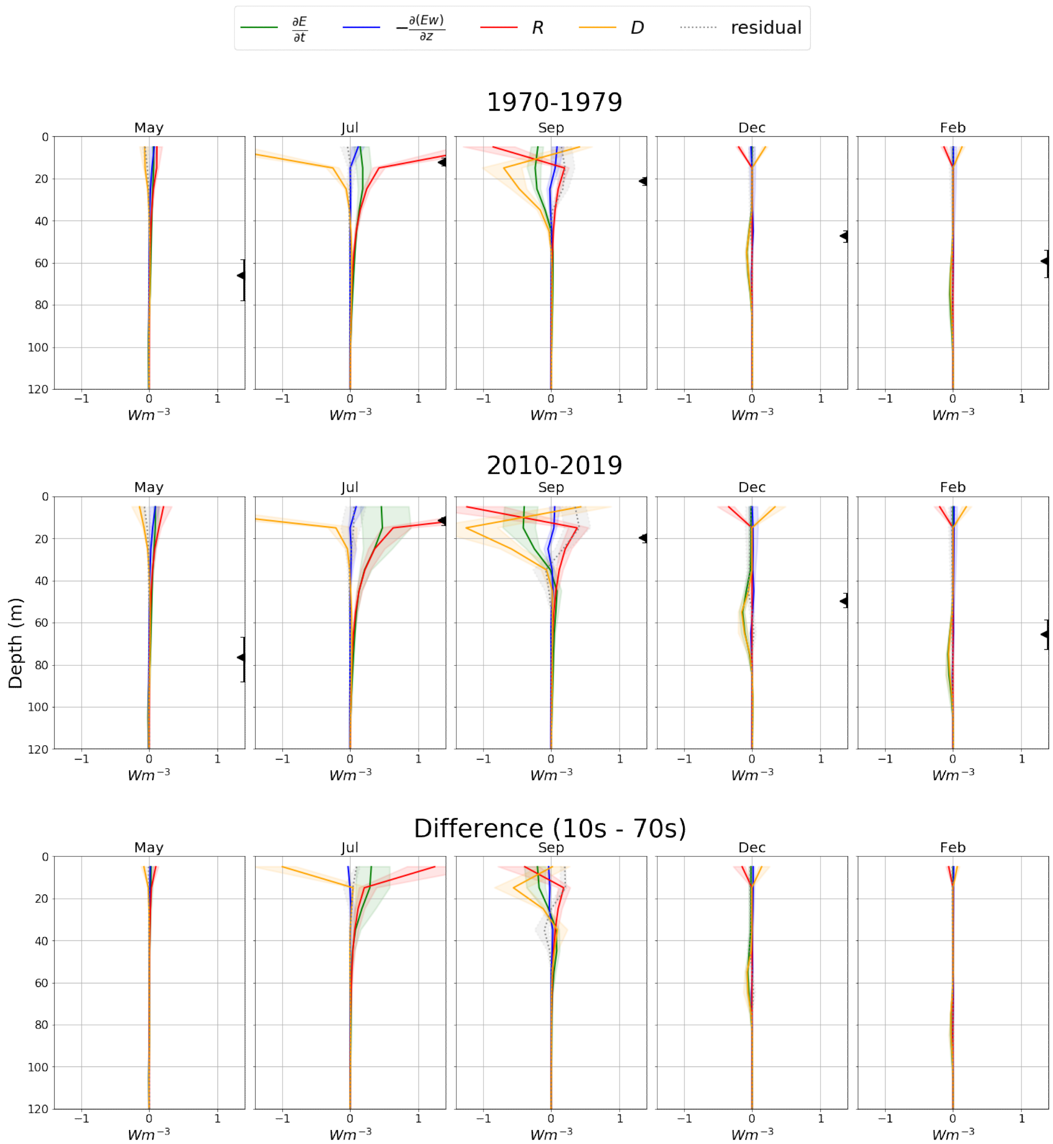

Figure 4.10: Estimated monthly vertical ocean heat budget using CESM-LE simulations of 1970-1979 (top), 2010-2019 (center), and their difference (bottom). The change in internal energy (green), divergence of surface fluxes (red), vertical diffusion (orange), vertical advection (blue), and the residual error (dotted grey) are indicated (see eq. 3.3 for details). The shaded region represents the basin-average maximum/minimum over the 40 ensemble members. Black trianges and errorbars indicate the basin-average mixed-layer depth and its maximum/minimum range. Note that the data for July exceeds the horizontal scale at 5 m in order to resolve fine-scale features in the winter. A positive value indicates that the process acts to increase heat and a negative value indicates that the process acts to decrease heat at a given depth.

We next show the decomposition of the diffusion flux in figure 4.11. In the summer, diabatic diffusion brings a little bit of heat from the halocline to the top layer. The ice-ocean turbulent flux transfers the heat from the top layer, mostly brought by shortwave flux, to the ice. In the fall, both diabatic and non-local diffusion remove heat from the halocline to bring it to the surface. In the winter, the ventilation of the NSTM is characterized by a double peak in diabatic diffusion that move heat upward and downward (the downward peak is not visible on this scale, see figure 4.11, cyan line). This heat brought upward reaches the bottom of the mixed layer where the non-local diffusion takes it to the surface.

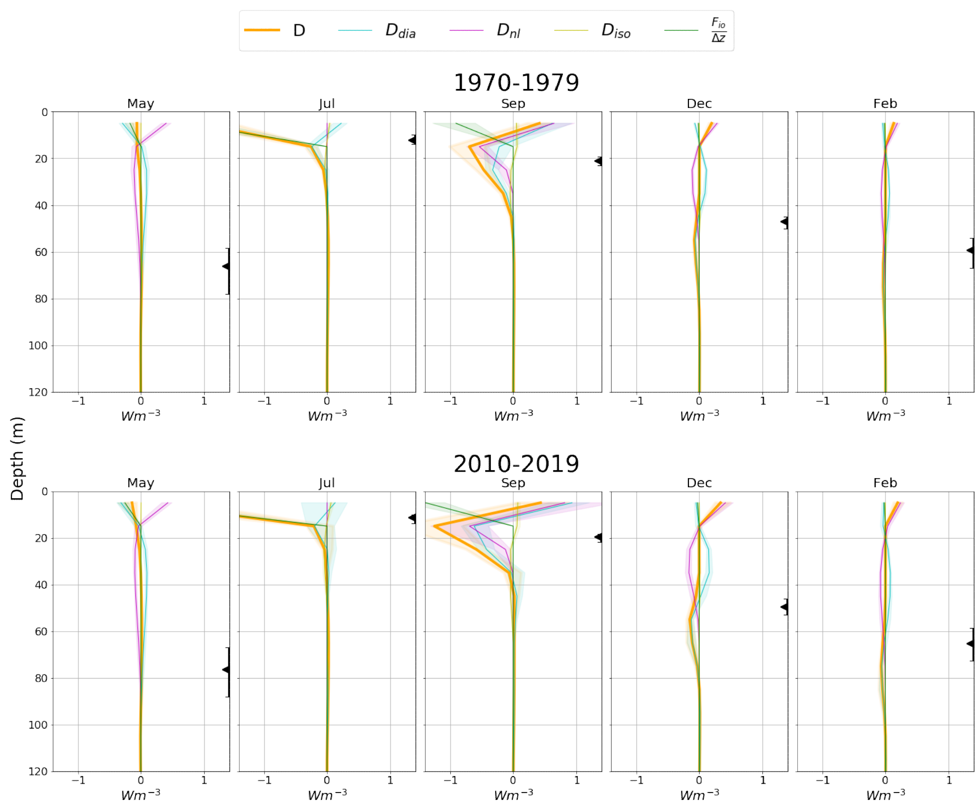

Figure 4.11: Simulated monthly change in heat from diffusive processes in 1970-1979 (top) and 2010-2019 (bottom). The total diffusion of heat (orange) occurs in response to the sum of the four processes: diabatic diffusion (cyan), non-local processes (pink), isopycnal diffusion (yellow), and ice-ocean turbulent heat flux (green). The shaded region represents the basin-average maximum/minimum over the 40 ensemble members.

To confirm our 1D assumption in the vertical heat budget, we calculate the residual and the portion of the residual of the 1D budget that is due to heat transport from horizontal processes (see figure 4.12). The budget has a very small residual from November to August. In the summer, the residual is quite small and can be mostly explained by horizontal heat fluxes. In the fall, the residual is larger, because there are larger temporal and spatial changes in internal heat leading to more error from the time discretization of the energy tendency term.

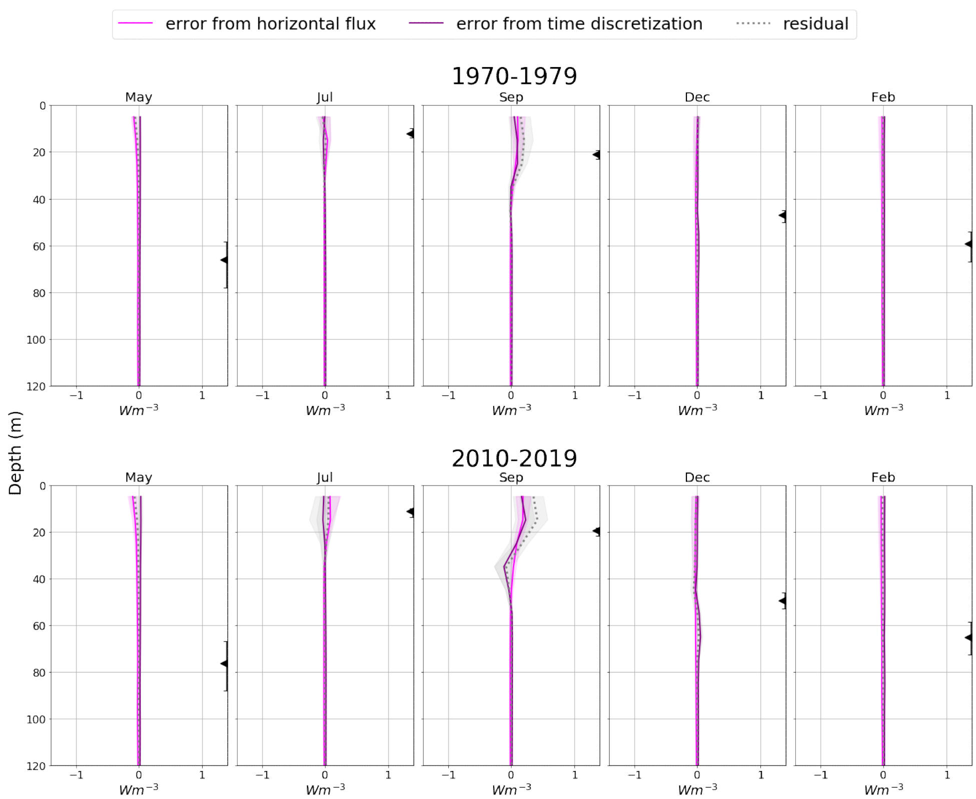

Figure 4.12: Simulated monthly decomposition of the residual in 1970-1979 (top) and 2010-2019 (bottom). This figure reproduces the residual from figure 4.10 (dotted grey line) and shows the part of the error that comes from heat tendency from horizontal flux (advection and diffusion) (pink). The error from the second order scheme of the energy time derivative (purple) is calculated as the difference between the residual and the horizontal contribution. The shaded region represents the maximum/minimum over the 40 ensemble members.

The vertical migration of heat is similar in 1970-1979 and 2010-2019, with larger heat fluxes in recent years (see the bottom row of figure 4.10). In July, there is more solar heat penetrating the ocean and, therefore, more heat stored in the ocean and more turbulent ice-ocean flux. However, the vertical diffusion of heat remains constant, similar to the vertical distribution of freshwater [Rosenblum et al., 2021a]. The input of heat to the ocean, through shortwave flux, increases, but the diffusion stays nearly the same. Hence, more heat is accumulated in the column. This extra heat will only be ventilated later in the year. There is more heat diffused upward from the halocline to the surface in 2010-2019 than in 1970-1979. This indicates that the extra heat accumulated in the ocean in recent years is mainly ventilated in the fall and winter.

The simulated biases related to the NSTM and PW will impact the vertical transport of heat in the ocean and the sea ice mass balance. The 2010-2019 NSTM is unrealistically cold and deep, implying that less heat will reach the surface. Further, the missing Pacific Water implies a missing vertical ocean heat flux that would lead to reduce ice formation in winter. The temperature gradient induced by the presence of Pacific Waters is similar or greater than the one associated with the NSTM (see figure 4.6). This provides a low bound estimate of the ocean heat flux from the vertical mixing of Pacific Waters in the CESM-LE (0.62 W m^{-3} for a 10 m layer thickness, the average heat brought to the top layer by diffusion), equivalent to 1.4 m of reduced winter ice growth over 3 years, the residence time in the Canada Basin [G.G. Campbell et al., 2021]. In the summer, the warm Pacific Waters are well below the seasonal pycnocline and are not believed to have a significant impact on the summer ice melt. This estimate is in the same order of magnitude as the 1.75 m of melt between 1980 and 2008 found by Kwok and Rothrock [2009]. Future work will be focused on a more precise estimation and will be calculated using a 1D column model of the vertical heat and salt transport constrained by observed vertical temperature and salinity profiles.

Chapter 5

Conclusion and Summary

We quantified changes to the seasonal vertical ice-ocean heat budget and sea ice mass balance between 1970-1979 and 2010-2019 in the Canada Basin using simulations from the CESM-LE. By examining the simulated transition from a seasonal to a perennial ice cover (pre and post-2000) and comparing with observations from 2004-2018 ITPs and 1975-1976 AIDJEX ice camps, we assess the reality of the simulated ocean heat transport.

First, we show that the summer ice-ocean heat budget is mainly balanced by the net shortwave radiation, the turbulent ice-ocean heat flux, and the internal heat change in the ocean. Compared to 1970-1979, the 2010-2019 ice-ocean turbulent flux and solar heat flux was $\sim$40% larger, contributing to a basal melt that was $\sim$60% larger. The net decrease in ice thickness was more moderate because of the increased in basal growth of 20% (the negative ice thickness – ice growth feedback).

Second, we found two main discrepancies between the model and the observations. The most striking difference is the complete absence of heat from Pacific Water in CESM-LE. By examining silicates, a tracer of Pacific Waters, we confirmed that the model incorrectly simulates the transport of Pacific Water into the Canada Basin. Instead, simulated PW follows the Alaskan coastline and is mostly entrained anticyclonically with the surface waters around Point Barrow. This is consistent with Zhang and Steele [2007], who showed that larger vertical diffusion increases the vertical extent of the surface anticyclonic circulation at the expense of the cyclonic at depth. The second large discrepancy – in opposition with observations showing an increased vertical stratification associated with ice melt as found by Peralta-Ferriz and Woodgate [2015] – is the increase in vertical mixing associated with a more mobile thinner pack ice despite increased surface freshwater fluxes associated with sea ice melt. This opposite process dominates in the CESM-LE, as the mixed layer depth is correctly represented in the 1970s but increases instead of decreasing as observed [Rosenblum et al., 2021b]. Again, this points to a problem in vertical mixing of the CESM-LE, consistent with previous studies [Holloway et al., 2007, Ilıcak et al., 2016, Rosenblum et al., 2021a]. Another change between the two periods that is not properly reproduced in the CESM-LE is the ventilation of the NSTM. In general, the NSTM has disappeared by May in the AIDJEX data and by December in the ITP data, but the CESM-LE shows an NSTM until May in both periods. We noted that there is large spatial and time variability by looking at individual AIDJEX camps and ITPs.

Third, a 1D budget of the vertical heat transport was presented. In general, the heat tendency from surface fluxes R is mirrored by the turbulent diffusion D. The vertical advection term is small compared to the other terms, even in the fall when the winds are strong and the pack-ice is still unconsolidated and mobile. This balance breaks down in the fall when the internal energy tendency term changes rapidly, which creates a larger error with the second-order differentiation scheme. In the summer, penetrating shortwave radiation warms the water column down to 80 m. Diabatic diffusion then takes heat in the seasonal halocline and brings it back to the surface, melting the ice. In the fall, diabatic diffusion takes heat accumulated in the mixed layer to the surface where it leaves through mostly sensible and longwave fluxes. In the winter, there is some remnant solar heat from the summer stored in the winter halocline. The diabatic diffusion brings it up to the bottom of the deep mixed layer and the non-local diffusion lifts it up to the surface where most of the heat leaves through the leads by sensible flux. Hence, the winter ocean remnant heat does not impede basal growth greatly, but stops new ice from forming in the leads. This balance does not go through large changes from the 1970s to the early 2000s. The amplitudes of all heat terms just get larger. Using this budget, a rough estimation was made that the missing Pacific Waters heat source would create $\sim$1.4 m of reduced winter ice growth over 3 years, a significant contribution, though a 1d model would be necessary to make a more accurate estimate. This will be the subject of future work.

Chapter 6

Appendix

Table 6.1: Names of the CESM-LE variables.

Variables	CESM-LE (POP)	CESM-LE (CICE)
Θ	TEMP	–
S	SALT	–
F_{hor}	ADVT + HDIFT	–
F_{io}	MELTH_F	fhocn_ai
F_{frazil}	QFLUX	–
F_{lw}	LWDN_F+LWUP_F	–
F_{sens}	SENH_F	–
F_{evap}	EVAP_F× latent_heat_vapor	–
$F_{sw}(z=0)$	SHF_QSW	–
$F_{sw,io}(z=0)$	–	fswthru_ai
$F_{sw,ao}(z=0)$	–	SHF_QSW
$F_{sw}(z)$	QSW_3D	–
$\frac{\partial h}{\partial t}\bigg\rvert_{\text{t}}$	–	−meltt
$\frac{\partial h}{\partial t}\bigg\rvert_{\text{b,l}}$	–	−meltb−meltl+congel
$\frac{\partial h}{\partial t}\bigg\rvert_{\text{f}}$	–	frazil
F_{ct}	–	fcondtop_ai
F_{cb}	–	−((congel−meltb−meltl)*rho_ice*latent_heat_fusion)
$F_{sw,ai}$	–	fswabs_ai
$F_{lw,ai}$	–	flwup_ai + (aice × flwdn)
$F_{sens,ai}$	–	fsens_ai
$F_{lat,ai}$	–	flat_ai
$w\Theta$	WTT Δz	–
$-\frac{\partial(wE)}{\partial z}$	$-\Delta$ WTT $c_p\rho$	–
$\frac{\partial}{\partial z}\kappa\frac{\partial\Theta}{\partial z}$	$\frac{\Delta\text{DIA\_IMPVF\_TEMP}}{\Delta z}$	–
$-\frac{\partial}{\partial z}\kappa\gamma_\Theta$	KPP_SRC_TEMP	–
$D_{iso}(\Theta)$	ΔHDIFB_TEMP	–

Bibliography

Knut Aagaard, L.K. Coachman, and Eddy Carmack. On the halocline of the Arctic Ocean. *Deep Sea Research Part A. Oceanographic Research Papers*, 28(6):529–545, June 1981. ISSN 01980149. doi: 10.1016/0198-0149(81)90115-1. URL `https://linkinghub.elsevier.com/retrieve/pii/0198014981901151`.

Gabriel Auclair and L. Bruno Tremblay. The Role of Ocean Heat Transport in Rapid Sea Ice Declines in the Community Earth System Model Large Ensemble. *Journal of Geophysical Research: Oceans*, 123(12):8941–8957, 2018. ISSN 2169-9291. doi: 10.1029/2018JC014525. URL `https://agupubs.onlinelibrary.wiley.com/doi/abs/10.1029/2018JC014525`. _eprint: https://agupubs.onlinelibrary.wiley.com/doi/pdf/10.1029/2018JC014525.

C. M. Bitz and William H. Lipscomb. An energy-conserving thermodynamic model of sea ice. *Journal of Geophysical Research: Oceans*, 104(C7):15669–15677, 1999. ISSN 2156-2202. doi: 10.1029/1999JC900100. URL `https://agupubs.onlinelibrary.wiley.com/doi/abs/10.1029/1999JC900100`. _eprint: https://agupubs.onlinelibrary.wiley.com/doi/pdf/10.1029/1999JC900100.

C. M. Bitz, M. M. Holland, A. J. Weaver, and M. Eby. Simulating the ice-thickness distribution in a coupled climate model. *Journal of Geophysical Research: Oceans*, 106 (C2):2441–2463, 2001. ISSN 2156-2202. doi: 10.1029/1999JC000113. URL `https:`

//agupubs.onlinelibrary.wiley.com/doi/abs/10.1029/1999JC000113. _eprint: https://agupubs.onlinelibrary.wiley.com/doi/pdf/10.1029/1999JC000113.

Tim P Boyer, Hernan E. Garcia, Ricardo A. Locarnini, Melisaa M. Zweng, Alexey V Mishonov, Jame R. Reagan, Katharine Weathers, Olga K. Baranova, Dan Seidov, and Igor V. Smolyar. World Ocean Atlas 2018, 2018. URL http://www.ncei.noaa.gov/products/world-ocean-atlas.

E. Carmack, I. Polyakov, L. Padman, I. Fer, E. Hunke, J. Hutchings, J. Jackson, D. Kelley, R. Kwok, C. Layton, H. Melling, D. Perovich, O. Persson, B. Ruddick, M.-L. Timmermans, J. Toole, T. Ross, S. Vavrus, and P. Winsor. Toward Quantifying the Increasing Role of Oceanic Heat in Sea Ice Loss in the New Arctic. *Bulletin of the American Meteorological Society*, 96(12):2079–2105, December 2015. ISSN 0003-0007. doi: 10.1175/BAMS-D-13-00177.1. URL https://journals.ametsoc.org/bams/article/96/12/2079/69295/Toward-Quantifying-the-Increasing-Role-of-Oceanic. Publisher: American Meteorological Society.

Judy Curry. SHEBA ISFF Flux-PAM Project Report | Earth Observing Laboratory, 1999. URL https://www.eol.ucar.edu/content/sheba-isff-flux-pam-project-report.

Peter E. D. Davis, Camille Lique, and Helen L. Johnson. On the Link between Arctic Sea Ice Decline and the Freshwater Content of the Beaufort Gyre: Insights from a Simple Process Model. *Journal of Climate*, 27(21):8170–8184, November 2014. ISSN 0894-8755, 1520-0442. doi: 10.1175/JCLI-D-14-00090.1. URL https://journals.ametsoc.org/view/journals/clim/27/21/jcli-d-14-00090.1.xml. Publisher: American Meteorological Society Section: Journal of Climate.

Peter E. D. Davis, Camille Lique, Helen L. Johnson, and John D. Guthrie. Competing Effects of Elevated Vertical Mixing and Increased Freshwater Input on the Stratification and Sea Ice Cover in a Changing Arctic Ocean. *Journal of Physical Oceanography*, 46 (5):1531–1553, May 2016. ISSN 0022-3670, 1520-0485. doi: 10.1175/JPO-D-15-0174.1. URL `https://journals.ametsoc.org/jpo/article/46/5/1531/342929/Competing-Effects-of-Elevated-Vertical-Mixing-and`.

Patricia DeRepentigny, L. Bruno Tremblay, Robert Newton, and Stephanie Pfirman. Patterns of Sea Ice Retreat in the Transition to a Seasonally Ice-Free Arctic. *Journal of Climate*, 29(19):6993–7008, October 2016. ISSN 0894-8755, 1520-0442. doi: 10.1175/JCLI-D-15-0733.1. URL `https://journals.ametsoc.org/view/journals/clim/29/19/jcli-d-15-0733.1.xml`. Publisher: American Meteorological Society Section: Journal of Climate.

Amélie Desmarais and Bruno Tremblay. Assessment of decadal variability in sea ice in the Community Earth System Model against a long-term regional observational record: implications for the predictability of an ice-free Arctic. *Journal of Climate*, -1(aop), February 2021. ISSN 0894-8755, 1520-0442. doi: 10.1175/JCLI-D-20-0561.1. URL `https://journals.ametsoc.org/view/journals/clim/aop/JCLI-D-20-0561.1/JCLI-D-20-0561.1.xml`. Publisher: American Meteorological Society Section: Journal of Climate.

Fetterer, F., Knowles K., Meier W., Savoie M., and Windnagel A. Sea Ice Index, Version 3, 2017. URL `https://nsidc.org/data/G02135/versions/3`. Type: dataset.

Peter R. Gent and James C. Mcwilliams. Isopycnal Mixing in Ocean Circulation Models. *Journal of Physical Oceanography*, 20(1):150–155, January 1990. ISSN 0022-3670, 1520-0485. doi: 10.1175/1520-0485(1990)020⟨0150:IMIOCM⟩2.0.CO;2. URL `https://journals.ametsoc.org/view/journals/phoc/20/1/`

1520-0485_1990_020_0150_imiocm_2_0_co_2.xml. Publisher: American Meteorological Society Section: Journal of Physical Oceanography.

G.G. Campbell, S. Pfirman, B. Tremblay, R. Newton, W. Meier, and C. Fowler. SITU | Sea Ice Tracking Utility. The Ice Tracker, 2021. URL http://icemotion.labs.nsidc.org/SITU/.

Donglai Gong and Robert S. Pickart. Summertime circulation in the eastern Chukchi Sea. *Deep Sea Research Part II: Topical Studies in Oceanography*, 118:18–31, August 2015. ISSN 0967-0645. doi: 10.1016/j.dsr2.2015.02.006. URL https://www.sciencedirect.com/science/article/pii/S096706451500034X.

H. Goosse, E. Deleersnijder, T. Fichefet, and M. H. England. Sensitivity of a global coupled ocean-sea ice model to the parameterization of vertical mixing. *Journal of Geophysical Research: Oceans*, 104(C6):13681–13695, 1999. ISSN 2156-2202. doi: https://doi.org/10.1029/1999JC900099. URL https://agupubs.onlinelibrary.wiley.com/doi/abs/10.1029/1999JC900099. _eprint: https://agupubs.onlinelibrary.wiley.com/doi/pdf/10.1029/1999JC900099.

G. Holloway, F. Dupont, E. Golubeva, S. Häkkinen, E. Hunke, M. Jin, M. Karcher, F. Kauker, M. Maltrud, M. A. Morales Maqueda, W. Maslowski, G. Platov, D. Stark, M. Steele, T. Suzuki, J. Wang, and J. Zhang. Water properties and circulation in Arctic Ocean models. *Journal of Geophysical Research: Oceans*, 112(C4), 2007. ISSN 2156-2202. doi: https://doi.org/10.1029/2006JC003642. URL https://agupubs.onlinelibrary.wiley.com/doi/abs/10.1029/2006JC003642. _eprint: https://agupubs.onlinelibrary.wiley.com/doi/pdf/10.1029/2006JC003642.

E. C. Hunke and J. K. Dukowicz. An Elastic–Viscous–Plastic Model for Sea Ice Dynamics. *Journal of Physical Oceanography*, 27(9):1849–1867, September 1997. ISSN 0022-3670, 1520-0485. doi: 10.1175/1520-0485(1997)027⟨1849:AEVPMF⟩2.0.

CO;2. URL https://journals.ametsoc.org/view/journals/phoc/27/9/1520-0485_1997_027_1849_aevpmf_2.0.co_2.xml. Publisher: American Meteorological Society Section: Journal of Physical Oceanography.

H. Huwald, L.-B. Tremblay, and H. Blatter. Reconciling different observational data sets from Surface Heat Budget of the Arctic Ocean (SHEBA) for model validation purposes. *Journal of Geophysical Research: Oceans*, 110(C5), 2005. ISSN 2156-2202. doi: https://doi.org/10.1029/2003JC002221. URL https://agupubs.onlinelibrary.wiley.com/doi/abs/10.1029/2003JC002221. _eprint: https://agupubs.onlinelibrary.wiley.com/doi/pdf/10.1029/2003JC002221.

Michael J. Iacono, Jennifer S. Delamere, Eli J. Mlawer, Mark W. Shephard, Shepard A. Clough, and William D. Collins. Radiative forcing by long-lived greenhouse gases: Calculations with the AER radiative transfer models. *Journal of Geophysical Research: Atmospheres*, 113(D13), 2008. ISSN 2156-2202. doi: 10.1029/2008JD009944. URL https://agupubs.onlinelibrary.wiley.com/doi/abs/10.1029/2008JD009944. _eprint: https://agupubs.onlinelibrary.wiley.com/doi/pdf/10.1029/2008JD009944.

Mehmet Ilıcak, Helge Drange, Qiang Wang, Rüdiger Gerdes, Yevgeny Aksenov, David Bailey, Mats Bentsen, Arne Biastoch, Alexandra Bozec, Claus Böning, Christophe Cassou, Eric Chassignet, Andrew C. Coward, Beth Curry, Gokhan Danabasoglu, Sergey Danilov, Elodie Fernandez, Pier Giuseppe Fogli, Yosuke Fujii, Stephen M. Griffies, Doroteaciro Iovino, Alexandra Jahn, Thomas Jung, William G. Large, Craig Lee, Camille Lique, Jianhua Lu, Simona Masina, A. J. George Nurser, Christina Roth, David Salas y Mélia, Bonita L. Samuels, Paul Spence, Hiroyuki Tsujino, Sophie Valcke, Aurore Voldoire, Xuezhu Wang, and Steve G. Yeager. An assessment of the Arctic Ocean in a suite of interannual CORE-II simulations. Part III: Hydrography and fluxes. *Ocean Modelling*, 100:141–161, April 2016. ISSN 1463-5003. doi: 10.1016/j.ocemod.

2016.02.004. URL https://www.sciencedirect.com/science/article/pii/S1463500316000238.

J. M. Jackson, E. C. Carmack, F. A. McLaughlin, S. E. Allen, and R. G. Ingram. Identification, characterization, and change of the near-surface temperature maximum in the Canada Basin, 1993–2008. *Journal of Geophysical Research: Oceans*, 115(C5), 2010. ISSN 2156-2202. doi: 10.1029/2009JC005265. URL https://agupubs.onlinelibrary.wiley.com/doi/abs/10.1029/2009JC005265. _eprint: https://agupubs.onlinelibrary.wiley.com/doi/pdf/10.1029/2009JC005265.

Jennifer M. Jackson, William J. Williams, and Eddy C. Carmack. Winter sea-ice melt in the Canada Basin, Arctic Ocean: WINTER SEA-ICE MELT CANADA BASIN. *Geophysical Research Letters*, 39(3):n/a–n/a, February 2012. ISSN 00948276. doi: 10.1029/2011GL050219. URL http://doi.wiley.com/10.1029/2011GL050219.

Alexandra Jahn, L. Bruno Tremblay, Robert Newton, Marika M. Holland, Lawrence A. Mysak, and Igor A. Dmitrenko. A tracer study of the Arctic Ocean's liquid freshwater export variability. *Journal of Geophysical Research: Oceans*, 115 (C7), 2010. ISSN 2156-2202. doi: 10.1029/2009JC005873. URL https://agupubs.onlinelibrary.wiley.com/doi/abs/10.1029/2009JC005873. _eprint: https://agupubs.onlinelibrary.wiley.com/doi/pdf/10.1029/2009JC005873.

E. P. Jones, J. H. Swift, L. G. Anderson, M. Lipizer, G. Civitarese, K. K. Falkner, G. Kattner, and F. McLaughlin. Tracing Pacific water in the North Atlantic Ocean. *Journal of Geophysical Research: Oceans*, 108(C4), 2003. ISSN 2156-2202. doi: https://doi.org/10.1029/2001JC001141. URL https://agupubs.onlinelibrary.wiley.com/doi/abs/10.1029/2001JC001141. _eprint: https://agupubs.onlinelibrary.wiley.com/doi/pdf/10.1029/2001JC001141.

J. E. Kay, C. Deser, A. Phillips, A. Mai, C. Hannay, G. Strand, J. M. Arblaster, S. C. Bates, G. Danabasoglu, J. Edwards, M. Holland, P. Kushner, J.-F. Lamarque, D. Lawrence, K. Lindsay, A. Middleton, E. Munoz, R. Neale, K. Oleson, L. Polvani, and M. Vertenstein. The Community Earth System Model (CESM) Large Ensemble Project: A Community Resource for Studying Climate Change in the Presence of Internal Climate Variability. *Bulletin of the American Meteorological Society*, 96(8):1333–1349, August 2015. ISSN 0003-0007, 1520-0477. doi: 10.1175/BAMS-D-13-00255.1. URL `https://journals.ametsoc.org/view/journals/bams/96/8/bams-d-13-00255.1.xml`. Publisher: American Meteorological Society Section: Bulletin of the American Meteorological Society.

Rachel Kim, Bruno Tremblay, Charles Brunette, and Robert Newton. A Regional Seasonal Forecast Model of Arctic Minimum Sea Ice Extent: Reflected Solar Radiation vs. Late Winter Coastal Divergence. *Journal of Climate*, -1(aop):1–1, May 2021. ISSN 0894-8755, 1520-0442. doi: 10.1175/JCLI-D-20-0846.1. URL `https://journals.ametsoc.org/view/journals/clim/aop/JCLI-D-20-0846.1/JCLI-D-20-0846.1.xml`. Publisher: American Meteorological Society Section: Journal of Climate.

R. Krishfield, J. Toole, A. Proshutinsky, and M.-L. Timmermans. Automated Ice-Tethered Profilers for Seawater Observations under Pack Ice in All Seasons. *Journal of Atmospheric and Oceanic Technology*, 25(11):2091–2105, November 2008. ISSN 0739-0572, 1520-0426. doi: 10.1175/2008JTECHO587.1. URL `https://journals.ametsoc.org/view/journals/atot/25/11/2008jtecho587_1.xml`. Publisher: American Meteorological Society Section: Journal of Atmospheric and Oceanic Technology.

R. Kwok and D. A. Rothrock. Decline in Arctic sea ice thickness from submarine and ICESat records: 1958–2008. *Geophysical Research Letters*, 36(15), 2009. ISSN 1944-8007. doi: https://doi.org/10.1029/2009GL039035. URL `https:`

//agupubs.onlinelibrary.wiley.com/doi/abs/10.1029/2009GL039035. _eprint: https://agupubs.onlinelibrary.wiley.com/doi/pdf/10.1029/2009GL039035.

C. Ladd, C. W. Mordy, S. A. Salo, and P. J. Stabeno. Winter Water Properties and the Chukchi Polynya. *Journal of Geophysical Research: Oceans*, 121(8):5516–5534, 2016. ISSN 2169-9291. doi: https://doi.org/10.1002/2016JC011918. URL https://agupubs.onlinelibrary.wiley.com/doi/abs/10.1002/2016JC011918. _eprint: https://agupubs.onlinelibrary.wiley.com/doi/pdf/10.1002/2016JC011918.

W. G. Large, J. C. McWilliams, and S. C. Doney. Oceanic vertical mixing: A review and a model with a nonlocal boundary layer parameterization. *Reviews of Geophysics*, 32(4):363–403, 1994. ISSN 1944-9208. doi: https://doi.org/10.1029/94RG01872. URL https://agupubs.onlinelibrary.wiley.com/doi/abs/10.1029/94RG01872. _eprint: https://agupubs.onlinelibrary.wiley.com/doi/pdf/10.1029/94RG01872.

William G. Large, Gokhan Danabasoglu, James C. McWilliams, Peter R. Gent, and Frank O. Bryan. Equatorial Circulation of a Global Ocean Climate Model with Anisotropic Horizontal Viscosity. *Journal of Physical Oceanography*, 31(2):518–536, February 2001. ISSN 0022-3670, 1520-0485. doi: 10.1175/1520-0485(2001)031⟨0518:ECOAGO⟩2.0.CO;2. URL https://journals.ametsoc.org/view/journals/phoc/31/2/1520-0485_2001_031_0518_ecoago_2.0.co_2.xml. Publisher: American Meteorological Society Section: Journal of Physical Oceanography.

P. Lemke and T. O. Manley. The seasonal variation of the mixed layer and the pycnocline under polar sea ice. *Journal of Geophysical Research: Oceans*, 89(C4):6494–6504, 1984. ISSN 2156-2202. doi: 10.1029/JC089iC04p06494. URL https://agupubs.onlinelibrary.wiley.com/doi/abs/10.1029/JC089iC04p06494. _eprint: https://agupubs.onlinelibrary.wiley.com/doi/pdf/10.1029/JC089iC04p06494.

Jed E. Lenetsky, Bruno Tremblay, Charles Brunette, and Gianluca Meneghello. Subseasonal Predictability of Arctic Ocean Sea Ice Conditions: Bering Strait and Ekman-Driven Ocean Heat Transport. *Journal of Climate*, 34(11):4449–4462, June 2021. ISSN 0894-8755, 1520-0442. doi: 10.1175/JCLI-D-20-0544.1. URL `https://journals.ametsoc.org/view/journals/clim/34/11/JCLI-D-20-0544.1.xml`. Publisher: American Meteorological Society Section: Journal of Climate.

B. P. Leonard. A stable and accurate convective modelling procedure based on quadratic upstream interpolation. *Computer Methods in Applied Mechanics and Engineering*, 19(1): 59–98, June 1979. ISSN 0045-7825. doi: 10.1016/0045-7825(79)90034-3. URL `https://www.sciencedirect.com/science/article/pii/0045782579900343`.

William H. Lipscomb. Remapping the thickness distribution in sea ice models. *Journal of Geophysical Research: Oceans*, 106(C7):13989–14000, 2001. ISSN 2156-2202. doi: 10.1029/2000JC000518. URL `https://agupubs.onlinelibrary.wiley.com/doi/abs/10.1029/2000JC000518`. _eprint: https://agupubs.onlinelibrary.wiley.com/doi/pdf/10.1029/2000JC000518.

T.O. Manley and K. Hunkins. Mesoscale eddies of the Arctic Ocean. *J. Geophys. Res.*, 90 (C3):4911–4930, 1985.

Douglas G. Martinson. Evolution of the southern ocean winter mixed layer and sea ice: Open ocean deepwater formation and ventilation. *Journal of Geophysical Research: Oceans*, 95(C7):11641–11654, 1990. ISSN 2156-2202. doi: https://doi.org/10.1029/JC095iC07p11641. URL `https://agupubs.onlinelibrary.wiley.com/doi/abs/10.1029/JC095iC07p11641`. _eprint: https://agupubs.onlinelibrary.wiley.com/doi/pdf/10.1029/JC095iC07p11641.

Wieslaw Maslowski, Jaclyn Clement Kinney, Matthew Higgins, and Andrew Roberts. The Future of Arctic Sea Ice. *Annual Review of Earth and Plan-*

etary Sciences, 40(1):625–654, May 2012. ISSN 0084-6597. doi: 10.1146/annurev-earth-042711-105345. URL https://www.annualreviews.org/doi/10.1146/annurev-earth-042711-105345. Publisher: Annual Reviews.

G. A. Maykut and Miles G. McPhee. Solar heating of the Arctic mixed layer. *Journal of Geophysical Research: Oceans*, 100(C12):24691–24703, 1995. ISSN 2156-2202. doi: 10.1029/95JC02554. URL https://agupubs.onlinelibrary.wiley.com/doi/abs/10.1029/95JC02554. _eprint: https://agupubs.onlinelibrary.wiley.com/doi/pdf/10.1029/95JC02554.

Gary A. Maykut and Norbert Untersteiner. Some results from a time-dependent thermodynamic model of sea ice. *Journal of Geophysical Research (1896-1977)*, 76(6):1550–1575, 1971. ISSN 2156-2202. doi: 10.1029/JC076i006p01550. URL https://agupubs.onlinelibrary.wiley.com/doi/abs/10.1029/JC076i006p01550. _eprint: https://agupubs.onlinelibrary.wiley.com/doi/pdf/10.1029/JC076i006p01550.

Fiona McLaughlin, Eddy Carmack, Andrey Proshutinsky, Richard Krishfield, Christopher Guay, Michiyo Yamamoto-Kawai, Jennifer Jackson, and Bill Williams. The Rapid Response of the Canada Basin to Climate Forcing: From Bellwether to Alarm Bells. *Oceanography*, 24(3):146–159, September 2011. ISSN 10428275. doi: 10.5670/oceanog.2011.66. URL https://tos.org/oceanography/article/the-rapid-response-of-the-canada-basin-to-climate-forcing-from-bellwether

Gianluca Meneghello, John Marshall, Jean-Michel Campin, Edward Doddridge, and Mary-Louise Timmermans. The Ice-Ocean Governor: Ice-Ocean Stress Feedback Limits Beaufort Gyre Spin-Up. *Geophysical Research Letters*, 45(20):11,293–11,299, 2018a. ISSN 1944-8007. doi: https://doi.org/10.1029/2018GL080171. URL https://agupubs.onlinelibrary.wiley.com/doi/abs/10.1029/2018GL080171. _eprint: https://agupubs.onlinelibrary.wiley.com/doi/pdf/10.1029/2018GL080171.

Gianluca Meneghello, John Marshall, Mary-Louise Timmermans, and Jeffery Scott. Observations of Seasonal Upwelling and Downwelling in the Beaufort Sea Mediated by Sea Ice. *American Meteorological Society*, April 2018b. ISSN 0022-3670. URL `https://dspace.mit.edu/handle/1721.1/118476`. Accepted: 2018-10-15T14:57:15Z Publisher: American Meteorological Society.

Gianluca Meneghello, Edward Doddridge, John Marshall, Jeffery Scott, and Jean-Michel Campin. Exploring the Role of the "Ice–Ocean Governor" and Mesoscale Eddies in the Equilibration of the Beaufort Gyre: Lessons from Observations. *Journal of Physical Oceanography*, 50(1):269–277, January 2020. ISSN 0022-3670, 1520-0485. doi: 10.1175/JPO-D-18-0223.1. URL `https://journals.ametsoc.org/view/journals/phoc/50/1/jpo-d-18-0223.1.xml`.

Eli J. Mlawer, Steven J. Taubman, Patrick D. Brown, Michael J. Iacono, and Shepard A. Clough. Radiative transfer for inhomogeneous atmospheres: RRTM, a validated correlated-k model for the longwave. *Journal of Geophysical Research: Atmospheres*, 102 (D14):16663–16682, 1997. ISSN 2156-2202. doi: 10.1029/97JD00237. URL `https://agupubs.onlinelibrary.wiley.com/doi/abs/10.1029/97JD00237`. _eprint: https://agupubs.onlinelibrary.wiley.com/doi/pdf/10.1029/97JD00237.

James Morison and J. Dungan Smith. Seasonal variations in the upper Arctic Ocean as observed at T-3. *Geophysical Research Letters*, 8(7):753–756, 1981. ISSN 1944-8007. doi: 10.1029/GL008i007p00753. URL `https://agupubs.onlinelibrary.wiley.com/doi/abs/10.1029/GL008i007p00753`. _eprint: https://agupubs.onlinelibrary.wiley.com/doi/pdf/10.1029/GL008i007p00753.

Moritz, Richard. Salinity, Temperature, Depth profiler data at AIDJEX stations April 1975 through April 1976, Version 1., 2020. URL `https://doi.org/10.34992/4xak-8r05`.

A. T. Nguyen, D. Menemenlis, and R. Kwok. Improved modeling of the Arctic halocline with a subgrid-scale brine rejection parameterization. *Journal of Geophysical Research: Oceans*, 114(C11), 2009. ISSN 2156-2202. doi: 10.1029/2008JC005121. URL https://agupubs.onlinelibrary.wiley.com/doi/abs/10.1029/2008JC005121. _eprint: https://agupubs.onlinelibrary.wiley.com/doi/pdf/10.1029/2008JC005121.

Anna Nikolopoulos, Robert S. Pickart, Paula S. Fratantoni, Koji Shimada, Daniel J. Torres, and E. Peter Jones. The western Arctic boundary current at 152°W: Structure, variability, and transport. *Deep Sea Research Part II: Topical Studies in Oceanography*, 56(17): 1164–1181, August 2009. ISSN 0967-0645. doi: 10.1016/j.dsr2.2008.10.014. URL https://www.sciencedirect.com/science/article/pii/S0967064508003445.

Guo-Yue Niu, Zong-Liang Yang, Robert E. Dickinson, and Lindsey E. Gulden. A simple TOPMODEL-based runoff parameterization (SIMTOP) for use in global climate models. *Journal of Geophysical Research*, 110(D21):D21106, 2005. ISSN 0148-0227. doi: 10.1029/2005JD006111. URL http://doi.wiley.com/10.1029/2005JD006111.

J. Carter Ohlmann. Ocean Radiant Heating in Climate Models. *Journal of Climate*, 16(9):1337–1351, May 2003. ISSN 0894-8755. doi: 10.1175/1520-0442-16.9.1337. URL https://journals.ametsoc.org/jcli/article/16/9/1337/30002/Ocean-Radiant-Heating-in-Climate-Models. Publisher: American Meteorological Society.

Cecilia Peralta-Ferriz and Rebecca A. Woodgate. Seasonal and interannual variability of pan-Arctic surface mixed layer properties from 1979 to 2012 from hydrographic data, and the dominance of stratification for multiyear mixed layer depth shoaling. *Progress in Oceanography*, 134:19–53, May 2015. ISSN 0079-6611. doi: 10.1016/j.pocean.2014.12.005. URL http://www.sciencedirect.com/science/article/pii/S0079661114002158.

D. K. Perovich, K. F. Jones, B. Light, H. Eicken, T. Markus, J. Stroeve, and R. Lindsay. Solar partitioning in a changing Arctic sea-ice cover. *Annals of Glaciology*, 52(57): 192–196, 2011a. ISSN 0260-3055, 1727-5644. doi: 10.3189/172756411795931543. URL https://www.cambridge.org/core/journals/annals-of-glaciology/article/solar-partitioning-in-a-changing-arctic-seaice-cover/363DD9F8A62A5D542B58B4C6D543E45D. Publisher: Cambridge University Press.

Donald K. Perovich and Jacqueline A. Richter-Menge. Regional variability in sea ice melt in a changing Arctic. *Philosophical Transactions of the Royal Society A: Mathematical, Physical and Engineering Sciences*, 373(2045):20140165, July 2015. doi: 10.1098/rsta.2014.0165. URL https://royalsocietypublishing.org/doi/full/10.1098/rsta.2014.0165. Publisher: Royal Society.

Donald K. Perovich, Bonnie Light, Hajo Eicken, Kathleen F. Jones, Kay Runciman, and Son V. Nghiem. Increasing solar heating of the Arctic Ocean and adjacent seas, 1979–2005: Attribution and role in the ice-albedo feedback. *Geophysical Research Letters*, 34(19), 2007. ISSN 1944-8007. doi: 10.1029/2007GL031480. URL https://agupubs.onlinelibrary.wiley.com/doi/abs/10.1029/2007GL031480. _eprint: https://agupubs.onlinelibrary.wiley.com/doi/pdf/10.1029/2007GL031480.

Donald K. Perovich, Jacqueline A. Richter-Menge, Kathleen F. Jones, and Bonnie Light. Sunlight, water, and ice: Extreme Arctic sea ice melt during the summer of 2007. *Geophysical Research Letters*, 35(11), 2008. ISSN 1944-8007. doi: 10.1029/2008GL034007. URL https://agupubs.onlinelibrary.wiley.com/doi/abs/10.1029/2008GL034007. _eprint: https://agupubs.onlinelibrary.wiley.com/doi/pdf/10.1029/2008GL034007.

Donald K. Perovich, Jacqueline A. Richter-Menge, Kathleen F. Jones, Bonnie Light, Bruce C. Elder, Christopher Polashenski, Daniel Laroche, Thorsten Markus, and Ronald Lindsay. Arctic sea-ice melt in 2008 and the role of solar heating. *Annals of Glaciology*, 52(57):355–359, 2011b. ISSN 0260-3055, 1727-5644. doi: 10.3189/172756411795931714. URL https://www.cambridge.org/core/journals/annals-of-glaciology/article/arctic-seaice-melt-in-2008-and-the-role-of-solar-heating/D897CF2FB0ABF20528C40976DA689B99. Publisher: Cambridge University Press.

Perovich, D., J. Richter-Menge, and C. Polashenski. Observing and understanding climate change: Monitoring the mass balance, motion, and thickness of Arctic sea ice, 2021. URL http://imb-crrel-dartmouth.org/archived-data/.

Algot K. Peterson, Ilker Fer, Miles G. McPhee, and Achim Randelhoff. Turbulent heat and momentum fluxes in the upper ocean under Arctic sea ice. *Journal of Geophysical Research: Oceans*, 122(2):1439–1456, 2017. ISSN 2169-9291. doi: https://doi.org/10.1002/2016JC012283. URL https://agupubs.onlinelibrary.wiley.com/doi/abs/10.1002/2016JC012283. _eprint: https://agupubs.onlinelibrary.wiley.com/doi/pdf/10.1002/2016JC012283.

Alek A. Petty, Jennifer K. Hutchings, Jacqueline A. Richter-Menge, and Mark A. Tschudi. Sea ice circulation around the Beaufort Gyre: The changing role of wind forcing and the sea ice state. *Journal of Geophysical Research: Oceans*, 121(5):3278–3296, 2016. ISSN 2169-9291. doi: https://doi.org/10.1002/2015JC010903. URL https://agupubs.onlinelibrary.wiley.com/doi/abs/10.1002/2015JC010903. _eprint: https://agupubs.onlinelibrary.wiley.com/doi/pdf/10.1002/2015JC010903.

Robert S. Pickart. Shelfbreak circulation in the Alaskan Beaufort Sea: Mean structure and variability. *Journal of Geophysical Research: Oceans*, 109(C4), April 2004. ISSN 0148-0227. doi: 10.1029/2003JC001912. URL https://agupubs.onlinelibrary.wiley.com/doi/full/10.1029/2003JC001912. Publisher: John Wiley & Sons, Ltd.

Robert S. Pickart, Thomas J. Weingartner, Lawrence J. Pratt, Sarah Zimmermann, and Daniel J. Torres. Flow of winter-transformed Pacific water into the Western Arctic. *Deep Sea Research Part II: Topical Studies in Oceanography*, 52(24):3175–3198, December 2005. ISSN 0967-0645. doi: 10.1016/j.dsr2.2005.10.009. URL `https://www.sciencedirect.com/science/article/pii/S096706450500216X`.

Andrey Proshutinsky, Richard Krishfield, Mary-Louise Timmermans, John Toole, Eddy Carmack, Fiona McLaughlin, William J. Williams, Sarah Zimmermann, Motoyo Itoh, and Koji Shimada. Beaufort Gyre freshwater reservoir: State and variability from observations. *Journal of Geophysical Research: Oceans*, 114(C1), 2009. ISSN 2156-2202. doi: 10.1029/2008JC005104. URL `https://agupubs.onlinelibrary.wiley.com/doi/abs/10.1029/2008JC005104`. _eprint: https://agupubs.onlinelibrary.wiley.com/doi/pdf/10.1029/2008JC005104.

Luc Rainville, Craig M. Lee, and Rebecca A. Woodgate. Impact of Wind-Driven Mixing in the Arctic Ocean. *Oceanography*, 24(3):136–145, 2011. ISSN 1042-8275. URL `https://www.jstor.org/stable/24861308`. Publisher: Oceanography Society.

Erica Rosenblum and Ian Eisenman. Sea Ice Trends in Climate Models Only Accurate in Runs with Biased Global Warming. *Journal of Climate*, 30(16):6265–6278, August 2017. ISSN 0894-8755, 1520-0442. doi: 10.1175/JCLI-D-16-0455.1. URL `https://journals.ametsoc.org/view/journals/clim/30/16/jcli-d-16-0455.1.xml`. Publisher: American Meteorological Society Section: Journal of Climate.

Erica Rosenblum, Robert Fajber, Julienne Stroeve, Sarah Gille, Bruno Tremblay, and Eddy Carmack. Surface salinity under transitioning ice cover in the Canada Basin: Climate model biases linked to vertical 2 distribution of freshwater. preprint, Oceanography, June 2021a. URL `http://www.essoar.org/doi/10.1002/essoar.10507260.1`.

Erica Rosenblum, Julienne Stroeve, Sarah T. Gille, L. Bruno Tremblay, Camille Lique, Robert Fajber, Ryan Galley, David Barber, Thiago Loureiro, and Jennifer Lukovich. Freshwater input and vertical mixing in the Canada Basin's seasonal halocline: 1975 vs 2006-2012, February 2021b. URL http://www.essoar.org/doi/10.1002/essoar.10507192.1. Archive Location: world Publisher: Earth and Space Science Open Archive Section: Oceanography.

B. Rudels, L. G. Anderson, and E. P. Jones. Formation and evolution of the surface mixed layer and halocline of the Arctic Ocean. *Journal of Geophysical Research: Oceans*, 101(C4):8807–8821, 1996. ISSN 2156-2202. doi: 10.1029/96JC00143. URL https://agupubs.onlinelibrary.wiley.com/doi/abs/10.1029/96JC00143. _eprint: https://agupubs.onlinelibrary.wiley.com/doi/pdf/10.1029/96JC00143.

William J. Shaw and Timothy P. Stanton. Vertical diffusivity of the Western Arctic Ocean halocline. *Journal of Geophysical Research: Oceans*, 119(8):5017–5038, 2014. ISSN 2169-9291. doi: 10.1002/2013JC009598. URL https://agupubs.onlinelibrary.wiley.com/doi/abs/10.1002/2013JC009598. _eprint: https://agupubs.onlinelibrary.wiley.com/doi/pdf/10.1002/2013JC009598.

Michael Steele and Timothy Boyd. Retreat of the cold halocline layer in the Arctic Ocean. *Journal of Geophysical Research: Oceans*, 103(C5):10419–10435, 1998. ISSN 2156-2202. doi: https://doi.org/10.1029/98JC00580. URL https://agupubs.onlinelibrary.wiley.com/doi/abs/10.1029/98JC00580. _eprint: https://agupubs.onlinelibrary.wiley.com/doi/pdf/10.1029/98JC00580.

Michael Steele, Jinlun Zhang, and Wendy Ermold. Mechanisms of summertime upper Arctic Ocean warming and the effect on sea ice melt. *Journal of Geophysical Research: Oceans*, 115(C11), 2010. ISSN 2156-2202. doi: https://doi.org/10.1029/2009JC005849. URL https://agupubs.

onlinelibrary.wiley.com/doi/abs/10.1029/2009JC005849. _eprint: https://agupubs.onlinelibrary.wiley.com/doi/pdf/10.1029/2009JC005849.

Michael Steele, Wendy Ermold, and Jinlun Zhang. Modeling the formation and fate of the near-surface temperature maximum in the Canadian Basin of the Arctic Ocean. *Journal of Geophysical Research: Oceans*, 116(C11), 2011. ISSN 2156-2202. doi: https://doi.org/10.1029/2010JC006803. URL https://agupubs.onlinelibrary.wiley.com/doi/abs/10.1029/2010JC006803. _eprint: https://agupubs.onlinelibrary.wiley.com/doi/pdf/10.1029/2010JC006803.

M.-L. Timmermans. The impact of stored solar heat on Arctic sea ice growth. *Geophysical Research Letters*, 42(15):6399–6406, 2015. ISSN 1944-8007. doi: 10.1002/2015GL064541. URL https://agupubs.onlinelibrary.wiley.com/doi/abs/10.1002/2015GL064541. _eprint: https://agupubs.onlinelibrary.wiley.com/doi/pdf/10.1002/2015GL064541.

M.-L. Timmermans, J. Toole, R. Krishfield, and P. Winsor. Ice-Tethered Profiler observations of the double-diffusive staircase in the Canada Basin thermocline. *Journal of Geophysical Research: Oceans*, 113(C1), 2008. ISSN 2156-2202. doi: https://doi.org/10.1029/2008JC004829. URL https://agupubs.onlinelibrary.wiley.com/doi/abs/10.1029/2008JC004829. _eprint: https://agupubs.onlinelibrary.wiley.com/doi/pdf/10.1029/2008JC004829.

J. M. Toole, M.-L. Timmermans, D. K. Perovich, R. A. Krishfield, A. Proshutinsky, and J. A. Richter-Menge. Influences of the ocean surface mixed layer and thermohaline stratification on Arctic Sea ice in the central Canada Basin. *Journal of Geophysical Research: Oceans*, 115(C10), 2010. ISSN 2156-2202. doi: https://doi.org/10.1029/2009JC005660. URL https://agupubs.onlinelibrary.wiley.com/doi/abs/10.1029/2009JC005660. _eprint: https://agupubs.onlinelibrary.wiley.com/doi/pdf/10.1029/2009JC005660.

N. Untersteiner. On the mass and heat budget of arctic sea ice. *Archiv für Meteorologie, Geophysik und Bioklimatologie Serie A*, 12(2):151–182, January 1961. ISSN 0066-6416, 1436-5065. doi: 10.1007/BF02247491. URL `http://link.springer.com/10.1007/BF02247491`.

Thomas Weingartner, Knut Aagaard, Rebecca Woodgate, Seth Danielson, Yasunori Sasaki, and Donald Cavalieri. Circulation on the north central Chukchi Sea shelf. *Deep Sea Research Part II: Topical Studies in Oceanography*, 52(24):3150–3174, December 2005. ISSN 0967-0645. doi: 10.1016/j.dsr2.2005.10.015. URL `https://www.sciencedirect.com/science/article/pii/S0967064505002158`.

Rebecca A. Woodgate, Tom Weingartner, and Ron Lindsay. The 2007 Bering Strait oceanic heat flux and anomalous Arctic sea-ice retreat. *Geophysical Research Letters*, 37 (1), 2010. ISSN 1944-8007. doi: https://doi.org/10.1029/2009GL041621. URL `https://agupubs.onlinelibrary.wiley.com/doi/abs/10.1029/2009GL041621`. _eprint: https://agupubs.onlinelibrary.wiley.com/doi/pdf/10.1029/2009GL041621.

M. Yamamoto-Kawai, F. A. McLaughlin, E. C. Carmack, S. Nishino, and K. Shimada. Freshwater budget of the Canada Basin, Arctic Ocean, from salinity, delta 18O, and nutrients. *Journal of Geophysical Research: Oceans*, 113(C1), 2008. ISSN 2156-2202. doi: https://doi.org/10.1029/2006JC003858. URL `https://agupubs.onlinelibrary.wiley.com/doi/abs/10.1029/2006JC003858`. _eprint: https://agupubs.onlinelibrary.wiley.com/doi/pdf/10.1029/2006JC003858.

Jinlun Zhang and Mike Steele. Effect of vertical mixing on the Atlantic Water layer circulation in the Arctic Ocean. *Journal of Geophysical Research: Oceans*, 112(C4), 2007. ISSN 2156-2202. doi: https://doi.org/10.1029/2006JC003732. URL `https://agupubs.onlinelibrary.wiley.com/doi/abs/10.1029/2006JC003732`. _eprint: https://agupubs.onlinelibrary.wiley.com/doi/pdf/10.1029/2006JC003732.